INFORMATION TO USERS

This manuscript has been reproduced from the microfilm master. UMI films the text directly from the original or copy submitted. Thus, some thesis and dissertation copies are in typewriter face, while others may be from any type of computer printer.

The quality of this reproduction is dependent upon the quality of the copy submitted. Broken or indistinct print, colored or poor quality illustrations and photographs, print bleedthrough, substandard margins, and improper alignment can adversely affect reproduction.

In the unlikely event that the author did not send UMI a complete manuscript and there are missing pages, these will be noted. Also, if unauthorized copyright material had to be removed, a note will indicate the deletion.

Oversize materials (e.g., maps, drawings, charts) are reproduced by sectioning the original, beginning at the upper left-hand corner and continuing from left to right in equal sections with small overlaps.

Photographs included in the original manuscript have been reproduced xerographically in this copy. Higher quality 6" x 9" black and white photographic prints are available for any photographs or illustrations appearing in this copy for an additional charge. Contact UMI directly to order.

Bell & Howell Information and Learning
300 North Zeeb Road, Ann Arbor, MI 48106-1346 USA
800-521-0600

UMI®

Université d'Ottawa · University of Ottawa

Wavelength-Dependent Polarization Dependent Loss and Polarization Mode Dispersion Measurements In Fiber-Optic Devices

By

Yihong Zhu

A thesis submitted to the

School of Graduate Studies and Research

in Partial fulfillment of the requirements for the degree of

Master of Applied Science

Ottawa-Carleton Institute for Electrical Engineering

School of Information Technology and Engineering

University of Ottawa

Ottawa, Ontario

September 22, 1999

Abstract

Polarization Mode Dispersion (PMD) is a fundamental characteristic of singlemode optical fibers and fiber-optic components that describes their propensity to split an optical signal into two orthogonal polarization modes with different propagation velocity, resulting in a different propagation time in each mode, called the differential group delay (DGD). Polarization Dependent Loss (PDL) refers to the maximum change in the power transmitted by an optical component or device as the input state of polarization (SOP) is varied over all possible polarization states. PMD and PDL combined are a major source of pulse distortion and spreading, and cause power fluctuations in a link that can increase the system bit error rate. The PDL and PMD of components must therefore be characterized accurately in order to assess the potential impact on the performance of next generation high-speed Dense Wavelength Division Multiplexing (DWDM) systems. The measurement of PDL/PMD, and especially the characterization of its wavelength dependence in wavelength selective optical components such as fiber gratings becomes critically important for system design and evaluation.

In the thesis, an overview of fiber gratings, including theoretical background, fabrication techniques and their applications in optical fiber telecommunication systems are presented to help the readers fully understand fiber gratings' properties, behavior, and the importance of their characterization. Three calculational tools, i.e., the Jones calculus, the Mueller calculus, and the Poincare sphere, as well as the concept of the principal state of polarization, are introduced to quantitatively describe the interaction of light with optical devices.

For the first time, the wavelength dependency of PDL in three types of fiber gratings commonly used in optical fiber communication systems: chirped fiber Bragg gratings for dispersion compensation, Wavelength Division Multiplexing (WDM) grating filters for add/drop multiplexing, and long period gratings for gain compensation, have been characterized. Three measurement set-ups for the Jones matrix method, the Mueller matrix method, and the polarization scanning method, have been implemented, and are discussed, compared and analyzed. Different calibration procedures were performed to account for the systems' PDL and the strong wavelength dependency of the setups. Typical measurement results in these fiber gratings and an uncertainty analysis are resented.

For PMD measurements, five PMD measurement techniques, the interferometric, the optical pulse, the Jones matrix eigenanalysis, the wavelength-scanning, and the modulation phase-shift methods were introduced. Two of them, i.e., the Jones matrix eigenanalysis and the interferometric methods used to characterize three types of fiber gratings, single-mode fiber spools and an optical circulator, are implemented and compared. Typical experimental results are presented, compared and discussed. An assessment of measurement uncertainties is presented for each of the techniques applied.

Acknowledgements

First of all, I would like to express my sincere appreciation to Dr. Eli Simova at National Research Council (NRC) and my thesis supervisor, Dr. Pierre Berini, for their various comments, constant guidance, support and encouragement throughout the course of this project.

Thanks also go to Dr. Grover at NRC for his comments and offering laboratory access at NRC, and Isabelle Jean of Sherbrooke University for help with the experimental setup for the Mueller matrix method.

I am also grateful to QPS Technologies, Montréal, Canada for supplying a variety of fiber gratings used in this work, and to CITO (Communications and Information Technology Ontario) Canada, for their financial support; and of course, my family for their support and encouragement.

Table Of Contents

Abbreviations

CSO - composite second order (distortion)

DGD - differential group delay

DOP - degree of polarization

DSF - dispersion-shifted fiber

DUT - device under test

DWDM - dense wavelength division multiplexing

EDFA - erbium-doped fiber amplifier

FBG - fiber Bragg grating

FWHM - full-width at half maximum

FWM - four-wave mixing

LED - light-emitting diode

OTDM - optical time division multiplexing

PDL - polarization dependent loss

PMD - polarization mode dispersion

PMF - polarization maintaining fiber

PSP - principal state of polarization

RSS - root sum of squares

SMF - singlemode fiber

SOP - state of polarization

SPM - self-phase modulation

UV - ultraviolet

List of Symbols

$\overline{\delta n_{eff}}$ ..... the "dc" index change spatially averaged over a grating period, p. 7.

v ..... the fringe visibility of the refractive index change, p. 7.

Λ ..... the nominal period of a grating, p. 7.

$\phi(z)$ ..... grating chirp at a position z, p. 7.

n_{core}, $n_{cladding}$ .... the refractive index in fiber core, cladding, p.8.

λ_B ..... the Bragg wavelength, p. 8.

n_{eff} ..... the effective refractive index, p.9.

A(z), B(z) ..... the forward- and backward- modes, respectively, p.9.

κ ..... the coupling coefficient, p.9.

$\hat{\sigma}$ ..... a general "dc" self-coupling coefficient, p.9

σ ..... a "dc" (period-averaged) coupling coefficient, p.9.

δ ..... the Bragg detuning parameter, p. 9;

the maximum allowable longitudinal angular step, p. 65.

γ ..... the maximum allowable latitudinal angular step, p. 65.

A_x, A_y and ϕ_x, ϕ_y ... the amplitude and phase of the two orthogonal electric field components, p. 34.

ω ..... the optical frequency

$\bar{\mathbf{J}}$ ..... known as the Jones vector

$\bar{\mathbf{J}}_{in}$, $\bar{\mathbf{J}}_{out}$ ..... the Jones vectors representing the input and output electric field, p. 36.

M ..... the Jones matrix, p. 36.

$\vec{S}$ ..... the Stokes parameters, p. 38.

S_0, S_1, S_2, S_3 ..... the four elements of a Stokes vector, p. 38.

s_1, s_2, s_3 ..... the normalized Stokes parameters, p. 38.

$\Delta = \phi_y - \phi_x$ .... the phase difference between the E-field components, p. 40.

E_x, E_y ..... electric field components along horizontal and vertical axes, p. 41.

$e^{\beta(\omega)}$ ..... complex propagation exponential, taking into account attenuation and absolute phase, p. 43.

$\varepsilon_{in,out}$ and $\phi_{in,out}$ ..... the amplitude and phase of the electric fields, p.44.

$\hat{\varepsilon}_{in,out}$ ..... complex unit vectors specifying the states of polarization.

$\vec{E}_{in,out}$ ..... the complex electric field components representing the input/output light, p. 44.

L ..... grating length or fiber length, p.9, p. 74.

T_{max}, T_{min} ..... the maximum, minimum power reflection or transmission through the device, p. 47.

P^{Cal} and P^{DUT} ..... the transmission/reflection power without the DUT (power calibration) and with the DUT, respectively, p. 48.

$S_i(\mathbf{J})$, i = 1, 2 ..... the singular values of the Jones matrix **J**, p. 51.

$\lambda_i(\mathbf{J}^{*t}\mathbf{J})$, i = 1, 2 ..... the eigen values of $\mathbf{J}^{*t}\mathbf{J}$, p. 51.

ε ..... the measurement uncertainty for the polarization-scanning method, p. 66.

δΔθ ..... the angle uncertainty in axis alignment between input and output light

$\delta\Delta\theta$ ..... the angle uncertainty in axis alignment between input and output light passing through the polarization controller, p.69.

$\Delta\tau$ ..... Differential delay between two polarization modes, p. 45.

l_c ..... mean coupling length, p. 73.

B ..... the average modal birefringence B, p. 73.

$\Delta\theta$ ..... the rotation about the PSP axis in radians, p. 74.

$\Delta\omega$ ..... the optical frequency change, p.74.

$<\Delta\tau>_\lambda$, $<\Delta\tau>_t$, or $<\Delta\tau>_T$ ..... the DGD averaged over wavelength, time, or temperature, p. 75.

ρ_1, ρ_2 ..... the eigenvalues of the product of $\mathbf{T}(\omega + \Delta\omega)\mathbf{T}^{-1}(\omega)$, p. 81.

$\Delta\lambda$ ..... the wavelength step, p. 81.

List of Figures

Chapter 1

Introduction

As we approach the turn of the century, we are witnessing explosive growth in the demand to transport large volumes of data, due to the proliferation of Internet and multimedia communications for business, education, and recreation. Not only is the per-user demand for bandwidth increasing by a factor of eight, but the number of users is rising rapidly [1]. As a result, communication networks have changed drastically, moving from microwave and satellite to fiber optic links.

Normally, there are two approaches for increasing optical network transmission capacity. One approach is the use of Optical Time Division Multiplexing (OTDM), a scheme that has the potential of increasing the bit rate for a single optical carrier to a value as high as 1 Tb/s. Another solution is achieved by employing Dense Wavelength Division Multiplexing (DWDM), in which data are transmitted at a lower bit rate over multiple wavelengths, or optical channels. The future high-speed networks will most likely combine the two approaches, increasing both the number of channels and the data rate per channel. Fiber gratings, acting as wavelength-selective reflection filters, have had an impact on the design of such systems. In some cases, devices with Bragg gratings offer the only cost effective solution for high-speed transmission.

The use of Erbium-Doped Fiber Amplifiers (EDFAs) solves the loss problem and makes possible ultra-long-distance optical transmission links. All links become dispersion-limited. Multi-mode and chromatic dispersion can be well managed and minimized by using dispersion compensation techniques, such as, using single mode fibers or dispersion-shifted fibers, narrow-linewidth DFB type lasers, and dispersion compensators in optical communication links. At higher bit rates (> 10 Gbit/s) with multiple optical channels, nonlinear effects, i.e., self-phase

modulation (SPM), cross-phase modulation (XPM), and four-wave mixing (FWM), as well as polarization effects, e.g, Polarization Mode Dispersion (PMD) and Polarization Dependent Loss (PDL) in fiber and fiber-optic devices, have now become major limiting factors.

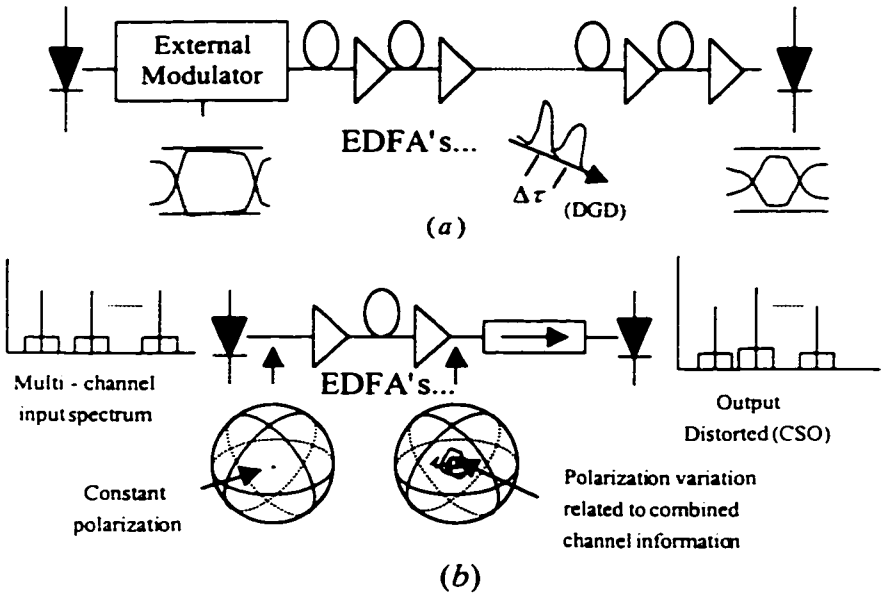

Figure 1-1. PMD and PDL can degrade performance of (a) along high-speed digital system and (b) a high channel-capacity CATV system [2].

PMD and PDL degrade the performance in long-haul high bit-rate fiber-optic communication links [3-5]. They cause jitter and closure of the eye-pattern and lead to interference effects which produces anomalously large optical pulse spreading [6] in digital communication links, as shown in Figure 1-1 (a), and therefore can increase the system bit error rate. PMD combined with PDL can also produce polarization-dependent intensity modulation and composite second order distortion (CSO) in an analog transmission link [3], as shown in Figure 1-1(b). PDL combined with PMD causes power fluctuations in a link that can increase system power penalty. SPM, XPM and FWM cause considerable spectral broadening of pulses

propagating inside the optical fiber, optical power loss, and interchannel crosstalk that degrades system performance [7-11]. In this thesis, PDL and PMD characterization and measurement techniques in fibers and fiber-optic components have been investigated.

1.1 Fiber Bragg Gratings (FBGs)

Accompanying the growing interest and deployment of fiber optic systems, with its emphasis on WDM transmission, is the development of new optical components/devices. Discoveries in optical transmitters, amplifiers, frequency converters, filters, and multiplexers provide new ways to generate, condition, and detect light. FBG filters [12-14] have received attention for their versatility and unique filtering capabilities.

A FBG is a periodic modulation of the refractive index along the fiber length induced by exposure of the fiber core to an intense optical interference pattern. Since the initial demonstration of fiber gratings, many approaches have been developed to write gratings directly into the core of the fiber. For non-side-writing technique (internal writing) [15], the period of a grating is fixed for a certain ultraviolet (UV) laser wavelength. Side-writing techniques, i.e., holographic [16], phase mask [17-19], point-by-point [20], etc., allow the fabrication of Bragg gratings at different wavelengths from the UV laser wavelength.

Fiber gratings have found many applications in lightwave communications. These applications include rare-earth doped fiber grating lasers [21], dispersion compensation [22], WDM demultiplexers [23], add/drop multiplexers [24], mode couplers [25], wavelength stabilization of laser diodes [26], hybrid fiber/semiconductor lasers [27], fiber amplifier gain control [28], grating-based sensors [29], time delays for phased array radar [30], nonlinear effect

switches [31], etc. With the development of DWDM networks, the characterization of polarization effects in fiber gratings becomes increasingly important.

1.2 PMD and PDL

It is well known that an ideal single-mode fiber with a perfectly cylindrical core of uniform diameter supports two orthogonally polarized modes that are degenerate. However, in real fibers, degeneracy between the orthogonally polarized fiber modes is removed due to the birefringence produced by core ellipticity or noncircularly symmetric stress [32].

The small difference in refractive index for a particular pair of orthogonal polarization states in singlemode fiber, called birefringence, originates from non-circularity of the fiber core in two ways: intrinsic and extrinsic, as shown in Figure 1-2.

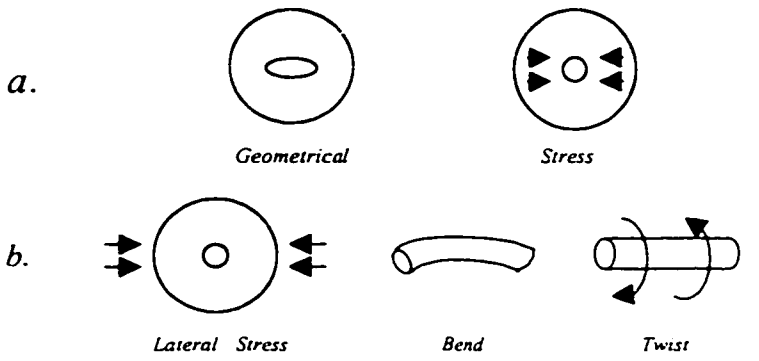

Figure 1-2. Intrinsic (a) and extrinsic (b) mechanisms of fiber birefringence [33].

The intrinsic birefringence is introduced in the manufacturing process, including a noncircular core and nonsymmetrical stress fields in the region around the core. The extrinsic sources of birefringence introduced in fiber spooling, cabling, or installation process, include lateral stress, bending and twisting. The birefringence, intrinsic and extrinsic, results in a difference in the propagation constants of the two orthogonal polarization modes. This

difference gives rise to a differential transit time, called the differential group delay (DGD), for the wave propagated in these polarization modes [34], referred as PMD. When the output pulse spreading becomes comparable to the bit time, the transmission performance degrades through intersymbol interference [5].

PDL is the maximum change in transmission/reflection with respect to polarization states. Many fiber-optic components, such as isolators, couplers, circulators, fiber gratings, exhibit PDL.

At any point along a fiber or fiber-optic component, the DGD is a deterministic value. However, in a long fiber or a passive optical network (PON) with concatenated optical components, PDL and PMD are random phenomena and their values have a statistical distribution dependent upon wavelength and the environment (temperature, vibration, etc.). Therefore, the characterization and measurement of PMD and PDL in fiber and fiber-optic components/devices are very important for optical system design and evaluation.

1.3 Organization

In this thesis, the wavelength dependent PDL and PMD in singlemode fiber and a variety of fiber-optic components are characterized. Different measurement techniques are implemented and compared. Typical experimental results are presented, compared, and discussed. An assessment of measurement uncertainties is presented for each of the techniques applied.

Chapter 2 gives an overview of fiber Bragg gratings, including the theoretical background, different fabrication techniques, and applications.

Chapter 3 gives a representation of polarized light and reviews Jones calculus, Stokes vector calculus (Mueller calculus), the Poincare sphere, and the Principal State of Polarization (PSP) required to understand and discuss PMD and PDL.

Chapter 4 is dedicated to PDL measurement techniques. Three experimental techniques i.e., the Jones matrix method, the Mueller matrix method and the polarization scanning method, are implemented and compared. Their theoretical background, experimental setups and measurement results in various fiber gratings are presented. Different calibration procedures are introduced to account for the system's PDL and strong wavelength dependence of the system components used. An assessment of measurement uncertainties is presented for each of the techniques applied.

Chapter 5 is dedicated to PMD measurement techniques. Five measurement techniques are introduced. Two of them, i.e., the Jones matrix eigen-analysis and the interferometric method are implemented and compared. Typical measurement results in fiber and fiber-optic components, as well as measurement-error analysis are presented.

Finally, Chapter 6 presents the conclusions and suggestions for future work.

Chapter 2

Overview of Fiber Gratings

An overview of fiber gratings is given in this chapter. First, the tools used to model fiber gratings are presented. Then, several different types of fiber gratings and three side-writing fabrication techniques are discussed. At the end, three kinds of applications using fiber gratings are presented.

2.1 Introduction

A fiber grating is a periodic modulation of the refractive index along the fiber length, as shown in Figure 2-1, induced by exposure of the fiber core to ultraviolet laser light. For simplicity, we can assume that the resulting perturbation is to the effective refractive index n_{eff} of the guided mode of interest, and can be described by:

$$\delta n_{eff}(z) = \overline{\delta n}_{eff}(z)\left\{1 + v\cos[\frac{2\pi}{\Lambda}z + \phi(z)]\right\} \qquad (2\text{-}1)$$

where $\overline{\delta n}_{eff}$ is the "dc" index change spatially averaged over a grating period, v is the fringe visibility of the index change, Λ is the nominal spatial period, and $\phi(z)$ describes the grating chirp [35].

Broadly, fiber gratings can be classified into two types: *Bragg gratings* (also called *reflection* and *short-period* gratings) and *transmission gratings* (also called *long-period* gratings). In Bragg gratings, the coupling is from a forward propagating guided mode to

backward propagating modes. In *transmission gratings*, the coupling is from a forward propagating guided mode to forward propagating cladding modes.

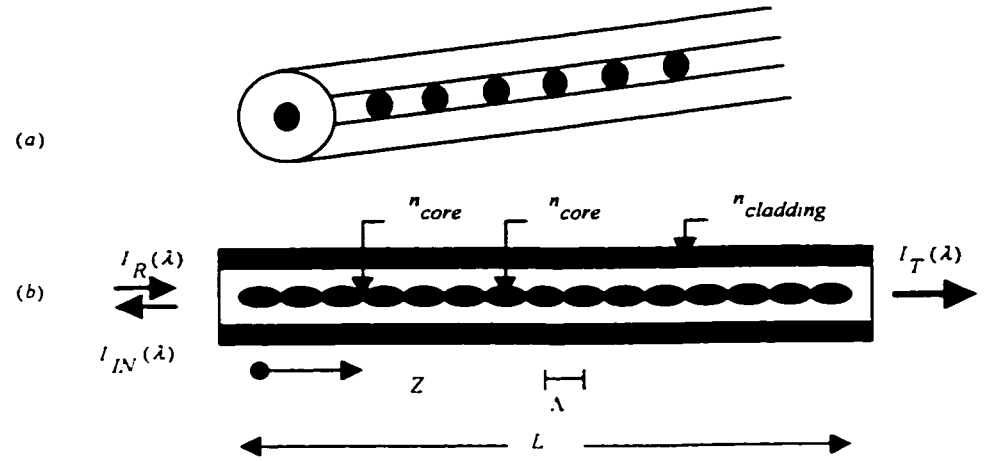

Figure 2-1. FBG illustrated (a) as a series of partially reflecting mirrors, (b) more accurately as a sinusoidal index modulation. L: grating length, Λ : grating period, n_{core} , $n_{cladding}$: the refractive index in fiber core, cladding.

The fiber grating characteristics can be modeled by several approaches [36-39]. Coupled-mode theory [40-42] is the foundation for most computations to obtain the spectral dependency and diffraction efficiency of fiber gratings, which is valid for small modulation depth.

2.1.1 **Fiber Bragg Gratings (FBGs)**

In FBGs, the dominant interaction is the coupling between the forward and backward propagating modes. The Bragg reflection occurs, if the period of the gating, Λ , referred as the period of the index perturbation, satisfies the Bragg condition at the stop band centered at the Bragg wavelength, λ_B :

$$\lambda_B = 2n_{eff}\Lambda . \tag{2-2}$$

The periodic nature of index variations couples the forward and backward propagating waves at wavelengths close to the Bragg wavelength. As a result, it provides wavelength-dependent reflectivity to the incident signal over a bandwidth determined by the grating strength, i.e. the depth of modulation of the refractive index, together with the grating period Λ and length L.

The equations describing this coupling can be written as [42]:

$$\begin{aligned} \frac{dR}{dz} &= i\hat{\sigma}R(z) + i\kappa S(z) \\ \frac{dS}{dz} &= -i\hat{\sigma}S(z) - i\kappa^{*}R(z) \end{aligned} , \tag{2-3}$$

where the amplitudes R and S are $R(z) \equiv A(z)\exp(i\delta z - \phi/2)$ and $S(z) \equiv B(z)\exp(-i\delta z + \phi/2)$. Here A(z) and B(z) denote the forward- and backward- modes, respectively, and κ is the coupling coefficient. A general "dc" self-coupling coefficient $\hat{\sigma}$ is defined as:

$$\hat{\sigma} \equiv \delta + \sigma - \frac{1}{2}\frac{d\phi}{dz} \tag{2-4}$$

where σ is a "dc" (period-averaged) coupling coefficient.

The Bragg detuning parameter δ is defined as:

$$\delta = \beta - \beta_B = 2\pi(\frac{1}{\lambda} - \frac{1}{\lambda_B}). \quad (2\text{-}5)$$

δ is a measure of the Bragg or phase mismatch between the modes. When the Bragg condition is met, δ is equal to zero and resonant mode coupling occurs, $\lambda = \lambda_B = 2n_{eff}\Lambda$. As δ increases, i.e. larger Bragg mismatching, mode coupling decreases to zero.

2.1.1.1 **Uniform FBGs**

A uniform grating is defined as having a sinusoidal index modulation with a constant or uniform average index along z. In this case, in Eqn. (2-1), $\overline{\delta n}_{eff}$ is a constant and $d\phi/dz = 0$. Therefore, κ, σ, and $\hat{\sigma}$ are constants. Thus Eqns. (2-3a) and (2-3b) are coupled first-order differential equations, and can be solved analytically with boundary conditions.

When resonance does occur, the maximum power reflectivity is given by [35]:

$$R_{\max} = I_R / I_{IN} = \tanh^2(\kappa L). \quad (2\text{-}6)$$

The bandwidth of the grating, defined as the distance between the first zeros in the reflection spectrum on either side of the peak reflectivity, is given by:

$$\Delta\lambda_{zero} = \lambda_B^2 / n_{eff} L \quad (2\text{-}7)$$

for a "weak" grating ($v\overline{\delta n}_{eff} << \lambda_B / L$), and

$$\Delta\lambda_{zero} = \lambda_B v\overline{\delta n}_{eff} / n_{eff} \qquad (2\text{-}8)$$

for a "strong" grating ($v\overline{\delta n}_{eff} >> \lambda_B / L$).

Thus in the weak grating case, the bandwidth is inversely proportional to length. This is a reasonable result since light will traverse more grating periods in a longer grating and have a narrower bandwidth reflection spectrum as a result of phase matching over a greater number of fringe planes. In the strong grating case, the bandwidth becomes independent of grating length and depends only on the index modulation. Light propagating through a strong grating is mostly reflected before it reaches the end of the grating, thus negating the full effect of the grating length.

Uniform gratings can function alone or in combination with other uniform gratings to act as narrowband transmission/reflection filters or bandpass filters for WDM, as shown in Figure 2-2.

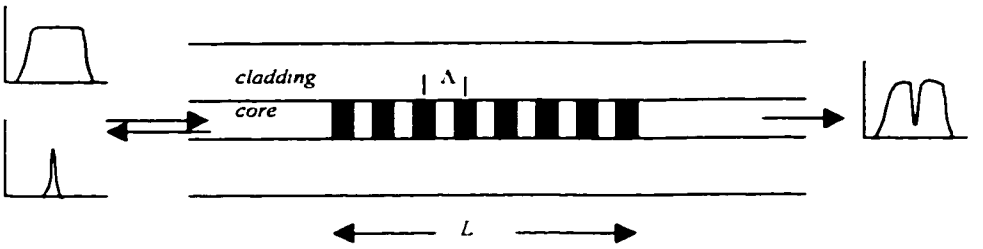

Figure 2-2. Schematic of a uniform grating illustrating the transmission and reflection spectrum response.

Typical examples of the power reflectivity for uniform gratings with κL=2 and κL=8 are shown in Figure 2-3 [35]. Large sidelobes can be observed.

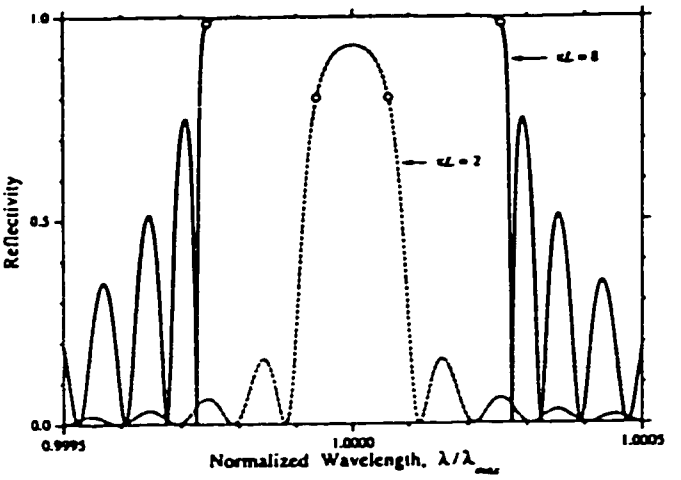

Figure 2-3. Reflection spectra versus normalized wavelength for Bragg reflection in uniform gratings with κ L=2 (dashed line) and κ L=8 (solid line) [35].

2.1.1.2 **Non-uniform FBGs**

The intensity profile of the laser beam used to write a fiber grating determines the index profile produced in the fiber. The index profile, in turn, determines the spectral characteristic of the grating. The reflection spectrum of a grating can thus be tailored by apodizing the writing beams to create a non-uniform grating.

The main reason for choosing a non-uniform design is to reduce the undesirable sidelobes prevalent in uniform grating spectra. There are also many other reasons to adjust the optical properties of fiber gratings by tailoring the grating parameters along the fiber axis. For example, chirping the period of a grating enables the dispersive properties of the scattered light to be tailored [36].

2.1.1.2.1 **Apodized Gratings**

An apodized non-uniform grating may be modeled by a raised cosine index modulation obtained by setting $\nu = 1, \phi = 0$ in Eqn. (2-1):

$$\delta n_{eff}(z) = \overline{\delta n}_{eff}(z)[1+\cos(\frac{2\pi}{\Lambda}z)] \tag{2-9}$$

where $\delta n_{eff}(z)$ is a spatially varying envelope function of the index perturbation [13].

$\overline{\delta n}_{eff}(z)$ usually takes the form of a Gaussian since an ultraviolet Gaussian beam is used to write the grating [43], thus:

$$\overline{\delta n}_{eff}(z) = \overline{\delta n}_{eff} \exp\left\{-4\ln 2\frac{z^2}{FWHM^2}\right\} \tag{2-10}$$

where FWHM denotes the full-width at half-maximum of the grating profile and $\overline{\delta n}_{eff}$ is the peak value of the "dc" effective index change.

In the uniform-grating model, the average index is independent of the grating strength and the peak of the grating reflection is centered at λ_B. In the apodized gratings, the increase in the average index with exposure causes a red shift in the grating spectrum. Since the index change is larger in the center of the grating, this portion is red-shifted by a greater amount than the rest of the gratings. As a result, it reflects light at a longer wavelength. The peak of the grating reflectivity (associated with the peak index) is shifted away from λ_B. The weaker parts of the grating, on the other hand, are not red shifted as much as the center of the grating and have their

local resonances at shorter wavelengths. A shorter wavelength is transparent to the center of the grating and is not reflected by it. As a result, effective Fabry-Perot cavities with resonance peaks on the short wavelength side of the peak reflectivity can be found, which can severely degrade resonant signal channels incident in an WDM add/drop filtering application.

To demonstrate the effects of apodization, Figure 2-4 shows the reflection and group delay versus wavelength for a grating similar to Figure 2-3, only here the grating has a Gaussian profile [35]. Bragg resonance peaks at THE shorter wavelength side can be observed.

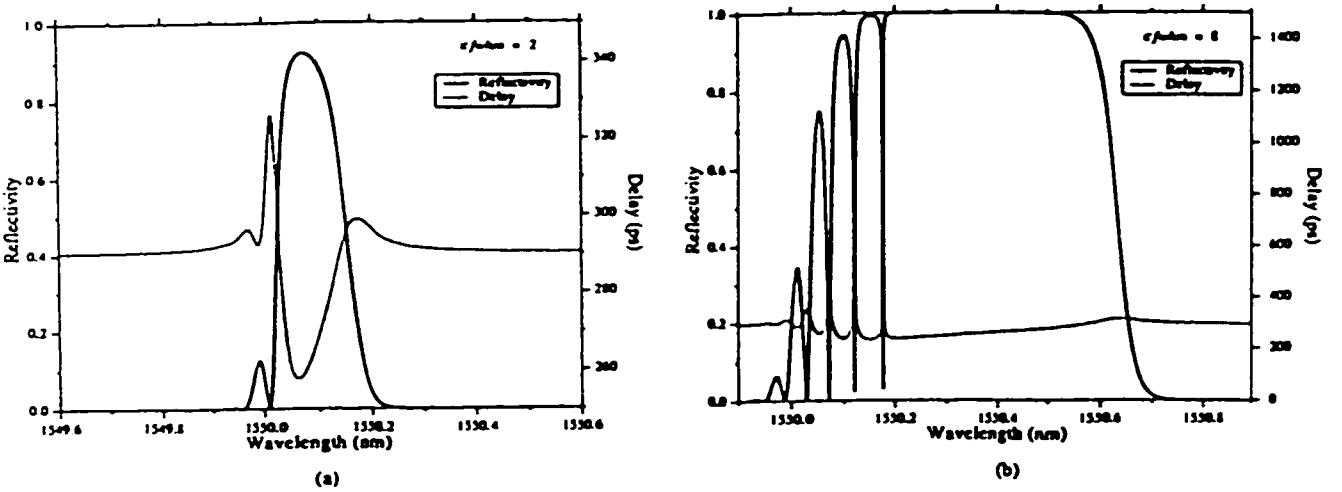

Figure 2-4. Reflection and group delay versus wavelength for Gaussian gratings similar to the uniform gratings in Figure 2-3: (a) κ FWHM = 2 and (b) κ FWHM = 8 [35].

2.1.1.2.2 Chirped FBGs

Uniform gratings usually have a relatively narrow stop band, the frequency region, in which most of the incident light is reflected back. However, a broadband grating is often

required in practice. Unlike a uniform grating that satisfies the Bragg condition for a specific wavelength, a chirped grating satisfies the Bragg condition for range of wavelengths. For a chirped FBG, the optical period, $n_{eff}\Lambda$, of the grating varies linearly over its length. Since the Bragg wavelength $\lambda_B = 2n_{eff}\Lambda$ also varies along the grating length, different frequency components of an incident optical pulse are reflected at different points, depending on where the Bragg condition is satisfied locally. The Bragg grating wavelength, λ_B, at an axial position z of an optical fiber Bragg grating is given by:

$$\lambda_B(z) = 2n_{eff}(z)\Lambda(z) \qquad (2\text{-}11)$$

where $n_{eff}(z)$ is the effective refractive index (averaged over the grating period) at position z, and $\Lambda(z)$ is the grating period at position z. Chirping can therefore be easily realized by axially varying Λ. Linear chirp can be specified in terms of a nonzero z-dependent phase term [35] $\frac{1}{2}\frac{d\phi}{dz} = -\frac{4\pi n_{eff}}{\lambda_B^2}\frac{d\lambda_B}{dz}$, or in terms of a dimensionless "chirp parameter", $F = \frac{\text{FWHM}^2}{z^2}\phi(z) = -4\pi n_{eff}\frac{\text{FWHM}^2}{\lambda_B^2}\frac{d\lambda_B}{dz}$ [36].

The piecewise-uniform approach is often preferred for modeling non-uniform gratings. This approach is based on identifying 2×2 matrices for each uniform section of the grating, and then multiplying all of these matrices together to obtain a single matrix that describes the whole grating, refer to [38].

Figure 2-5 shows the measured reflectivity and the time delay for the apodized and linearly chirped grating [44].

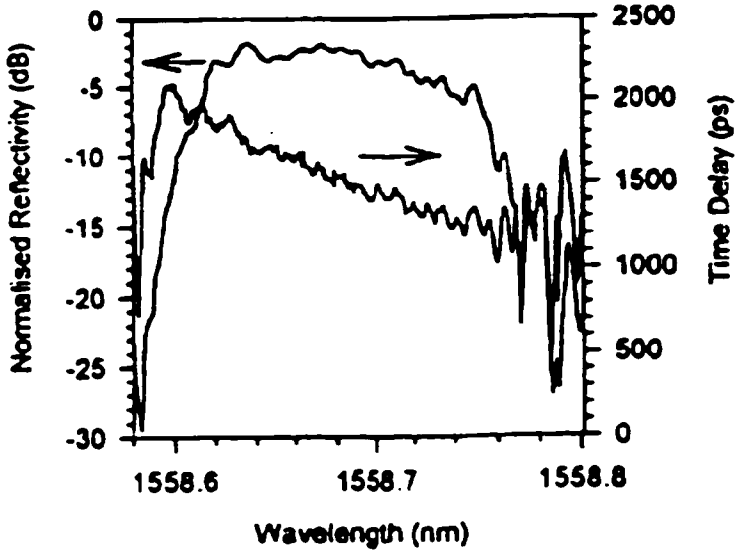

Figure 2-5. Measured reflectivity and time delay for a 10-cm-long, apodized and linearly chirped, fiber grating having a bandwidth of 0.12 nm. The slope of the linear time delay is a measure of the dispersion-compensation capability of the grating [44].

2.1.2 **Transmission Gratings (Long Period Gratings)**

If the grating period is much longer than the writing wavelength, referred to as a long-period ($\Lambda >> \lambda$) grating, light from a guided fundamental mode of amplitude $A_1(z)$ can be coupled in to a forward propagating cladding mode of amplitude $A_2(z)$. As they travel along the axis of the fiber, these modes have a tendency to decay rapidly over a short distance, mainly as a result of absorption and scattering at the cladding-coating interface.

The equations describing this coupling can be written by:

$$\frac{dR}{dz} = i\hat{\sigma}R(z) + i\kappa S(z)$$
$$\frac{dS}{dz} = -i\hat{\sigma}S(z) + i\kappa^{*}R(z) \qquad (2\text{-}12)$$

where the amplitudes R and S are $R(z) \equiv A_1 \exp[-i(\sigma_{11} + \sigma_{22})z/2]\exp(i\delta z - \phi/2)$ and $S(z) \equiv A_2 \exp[-i(\sigma_{11} + \sigma_{22})z/2]\exp(-i\delta z + \phi/2)$. Here σ_{11} and σ_{22} are "dc" coupling coefficients [42]. $*/\kappa = \kappa_{21} = \kappa_{12}^{*}$ is the "ac" cross-coupling coefficient and $\hat{\sigma}$ is a general "dc" self-coupling coefficient defined as:

$$\hat{\sigma} = \delta + \frac{\sigma_{11} - \sigma_{12}}{2} - \frac{1}{2}\frac{d\phi}{dz}. \qquad (2\text{-}13)$$

The detuning, assumed to be constant along z, is given by:

$$\delta = \frac{1}{2}(\beta_1 - \beta_2) - \frac{\pi}{\Lambda} = \pi\Delta n_{eff}\left(\frac{1}{\lambda} - \frac{1}{\lambda_B}\right) \qquad (2\text{-}14)$$

where $\lambda_B = \Delta n_{eff}\Lambda$ is the design wavelength for weak guiding. When the Bragg condition is met, δ is equal to zero and resonant mode coupling occurs, $\lambda = \lambda_B = \Delta n_{eff}\Lambda$. As δ increases, i.e. larger Bragg mismatching, mode coupling decreases to zero.

Figure 2-6 shows a typical transmission spectrum for long period fiber gratings. Since the coupling to the cladding modes is wavelength dependent, the long period fiber grating acts as a wavelength-selective loss device and can be used in the gain flattening of EDFAs.

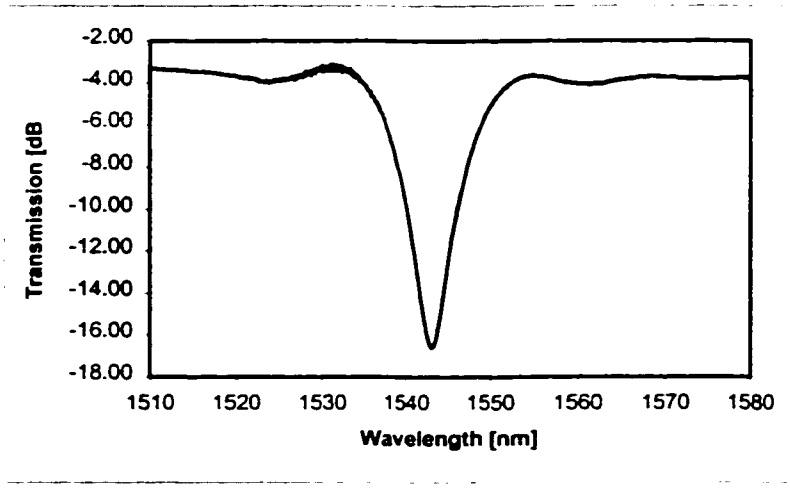

Figure 2-6. Typical transmission spectrum through long period gratings.

2.1.3 Tilted Gratings (Blazed Gratings)

Tilted/blazed gratings have grating fringes tilted at an angle to the fiber axis [45, 46]. The main effect of grating tilt in a single-mode Bragg grating is to effectively reduce the fringe visibility, and couple light in the fiber core to radiation modes outside the fiber core.

Assume that the induced index change in the core of the fiber is given by:

$$\delta n_{core}(x,z) = \overline{\delta n}_{core}(z')\{1 + v\cos[\frac{2\pi}{\Lambda g}z' + \phi(z')]\} \qquad (2\text{-}15)$$

where $\overline{\delta n}_{core}$ is the "dc" index change in the fiber core. Here the z' axis, as shown in Figure 2-7, is defined as $z' = x\sin\theta + z\cos\theta$. The grating period along the z (fiber) axis is $\Lambda = \Lambda_g / \cos\theta$. For the slowly varying functions $\overline{\delta n}_{core}(z')$ and $\varphi(z')$, we have $z' \cong z\cos\theta$, simply taking the projection of these functions onto the fiber axis.

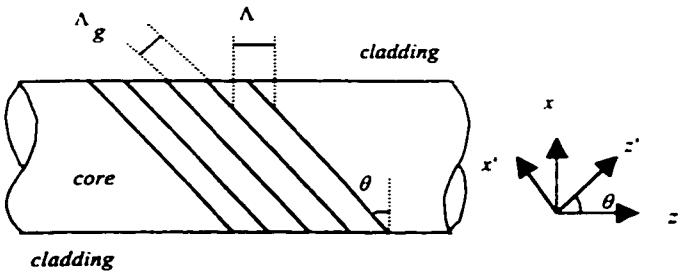

Figure 2-7. Diagram of the parameters associated with a tilted phase grating in the core of an optical fiber.

The tilt of the grating planes and strength of the photo-refractivity determines the coupling efficiency and bandwidth of the light that is tapped out. In tilted short-period ($\Lambda < \lambda$) gratings, the coupling is from a forward propagating guided-mode to backward propagating modes. A schematic diagram of a blazed grating used for flattening the input spectrum is shown in Figure 2-8. Figure 2-9 shows the calculated reflectivity spectrum over a range of tilt angles for a Gaussian grating with a FWHM = 5 mm [35].

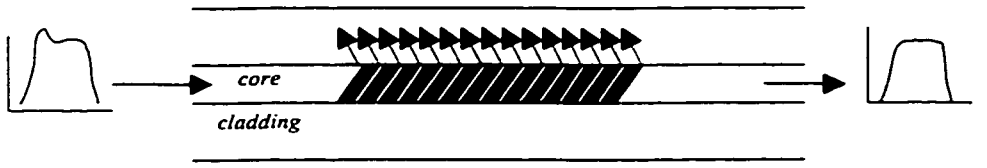

Figure 2-8. Schematic diagram of a blazed grating illustrating the flattening of the input spectrum.

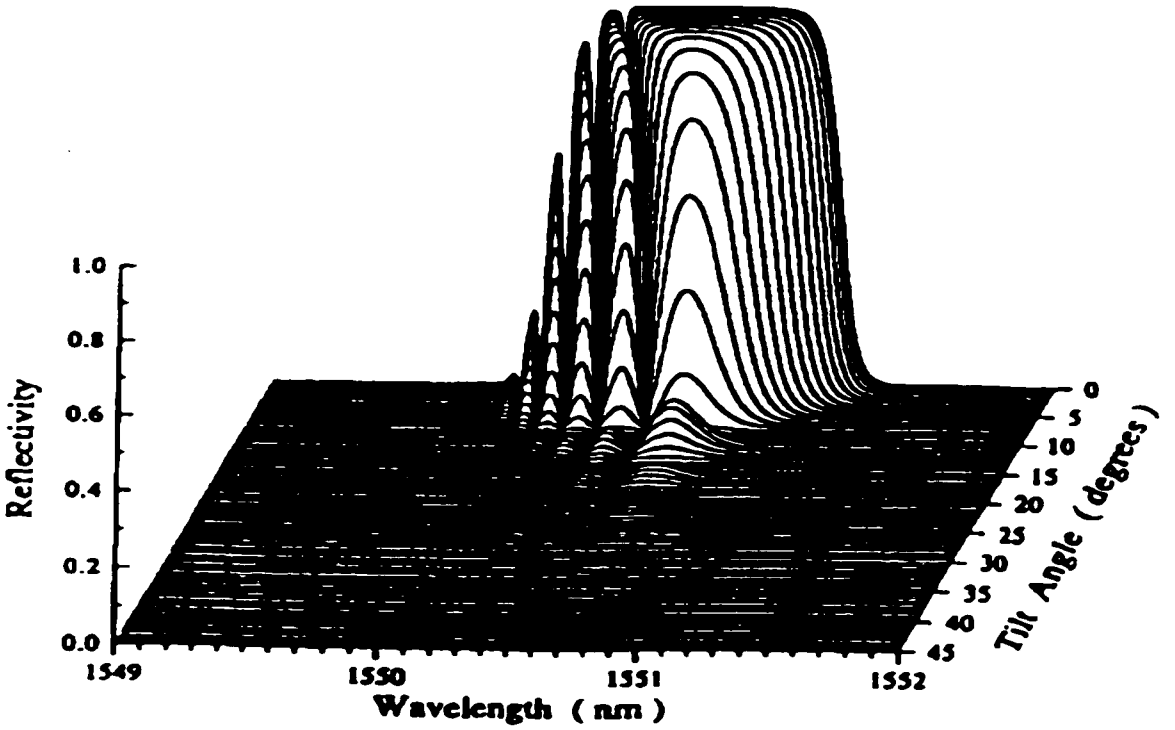

Figure 2-9. Calculated reflectivity spectrum over a range of grating tilt angles for a Gaussian grating [35].

2.2 Fabrication Techniques

Since 1978, when K. O. Hill and his colleagues first observed a photoinduced grating in a germania-doped optical fiber [12], many approaches have been developed to write gratings directly into the core of the fiber.

For non-side-writing techniques (internal writing) [12, 15], the period of a grating is fixed for certain UV laser wavelength used.

Another major approach in grating technology is the side-writing technique, transverse exposure on the side of the fiber with an interference pattern formed with an intense UV laser

source to produce the index modulation or phase grating in the fiber core [16]. Side-writing (transverse) techniques, i.e. holographic, phase mask [17-19], point-by-point [20,47], etc., allow fabrication of Bragg gratings at different wavelengths from the UV laser wavelength.

The transverse approach allows for the fabrication of gratings with essentially any spacing or Bragg resonance wavelength. The gratings could also be written at any desired location along the fiber with different exposure lengths and beam profiles to control the Bragg resonance spectrum.

2.2.1 Photoinduced Process

Photosensitivity in optical fiber is defined as the permanent change in the refractive index within the fiber due to laser exposure, usually in UV. Fiber can be rendered photosensitive by doping the core with germanium, phosphorous, or boron during fabrication of the preform. Fibers can also be sensitized by loading them with hydrogen under temperature and/or pressure, that is, by putting them in a chamber pressurized with hydrogen. However, the hydrogen-loading technique yields variable results and is not considered suitable for mass production.

Even though there has been considerable interest and activity in fiber grating technology, the physical mechanisms underlying photosensitivity are not completely understood. It is suspected that more than one process is involved in the grating formation dynamics. Basically, the inducing radiation breaks certain bonds in the glass structure like the oxygen-vacancy-defect bonds in germania-doped silica. Electrons are set free and find their way to color center traps elsewhere in the structure. Annealing experiments indicate that there may be two or more traps with different ranges of energies [48]. The new electron traps change the absorption properties of the doped silica, principally in the UV portion of the spectrum. The positive net change in the

relationships [49]. Other effects, such as the relief of induced stress and/or configurational changes in the structure of the fiber core material when the bonds are photolytically broken by the radiation, may also play a significant role in the induced index change.

2.2.2 Side-Writing Techniques

2.2.2.1 Holographic side-writing technique

First introduced by G. Meltz [16], the holographic side writing method used a split beam interferometer which is similar to that shown in Figure 2-10. Two beams intersect at the fiber producing a periodic interference pattern that is recorded in the core as a refractive index modulation with period:

$$\Lambda = \lambda / \{2\sin(\theta)\} . \tag{2-15}$$

Cylindrical lenses are placed in the interferometer to focus the interfering beams to a line image on the fiber. This produces a greater intensity interference pattern on the core and reduces exposure time. An additional turning mirror can be placed in one arm of the interferometer to remove the mirror symmetry of the reflections as shown in the figure. The Bragg wavelength is given by:

$$\lambda_B = 2n_{eff}\Lambda = n_{eff}\left(\frac{\lambda}{\sin\theta}\right). \tag{2-16}$$

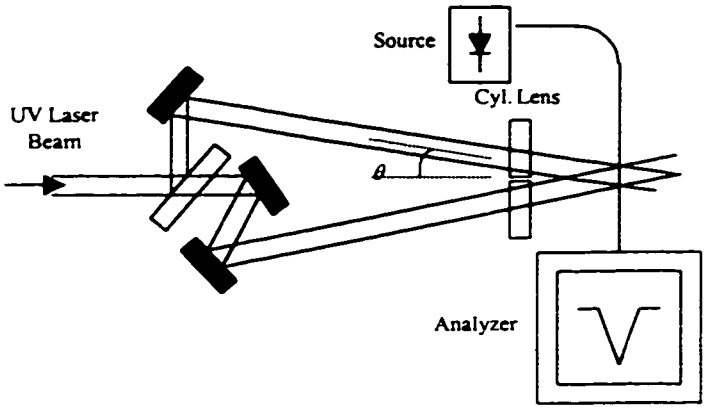

Figure 2-10. Two-beam interferometer for side-writing fiber Bragg gratings.

Therefore, the grating periodicity can be controlled simply by changing the angle θ or by changing the laser wavelength λ within the absorption band. However, the interferometer is susceptible to mechanical vibrations and air currents. The holographic technique is also critical to setup and alignment, since it is difficult to set precise angle and the repeatability of the Bragg wavelength λ_B is low. The laser must have a very good spatial and temporal coherence.

An alternative holographic approach is the prism technique shown in Figure 2-11. The prism acts as a common path interferometer making it an inherently more stable arrangement. The illuminating laser beam is incident on the prism hypotenuse. This input is oriented so that half the beam is reflected off the back face of the prism and interferes with the other half of the beam that is refracted directly to the bottom of the prism. One disadvantage of this approach is that the folded beam produces a " half Gaussian" index profile in the fiber that can create strong sidelobes in the reflection spectrum [50].

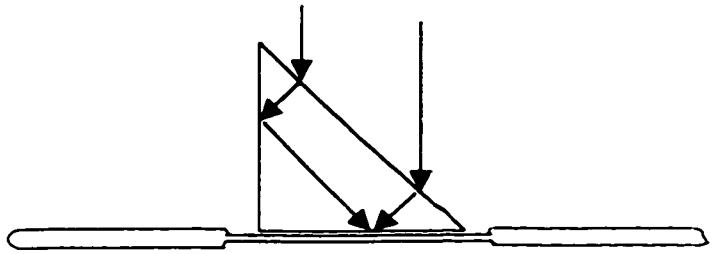

Figure 2-11. Side-writing technique: prism.

2.2.2.2 **Point-by-point technique**

The point-by-point approach, shown in Figure 2-12, was developed at the Communication Research Centre (CRC) Canada [20,47]. In this method, a writing beam is pulsed as the fiber is translated so that the individual grating lines may be written into the fiber. The input beam must thus be tightly focused. Also, the process is slow and requires high precision translation. Longer period gratings for mode couplers, rocking filters and even higher order Bragg gratings can be made point-by-point using precision translation stages.

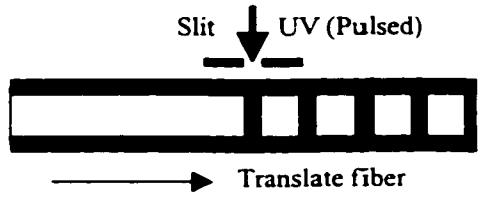

Figure 2-12. Fiber Bragg grating fabrication with point-by-point technique.

2.2.2.3 **Side-writing with phase mask**

The phase mask technique is gaining recognition over the holographic [16] and point-by-point [47] techniques of writing Bragg gratings due to its simplicity and reduced mechanical sensitivity. Very precise gratings can be formed by using an electron-beam phase mask and either an argon fluoride (193 nm) or krypton fluoride (248 nm) excimer laser as the UV source.

A phase mask is essentially a binary grating in which the groove profile and depth have been specially tailored to diffract most of the incident UV energy into the plus and minus first-diffraction orders while minimizing the energy in the zero and higher orders. Fabrication by electron-beam lithography ensures a high degree of accuracy in the mask period. During fiber-grating fabrication, the laser-illuminated phase mask diffracts incident UV light into the various diffraction orders, see Figure 2-13.

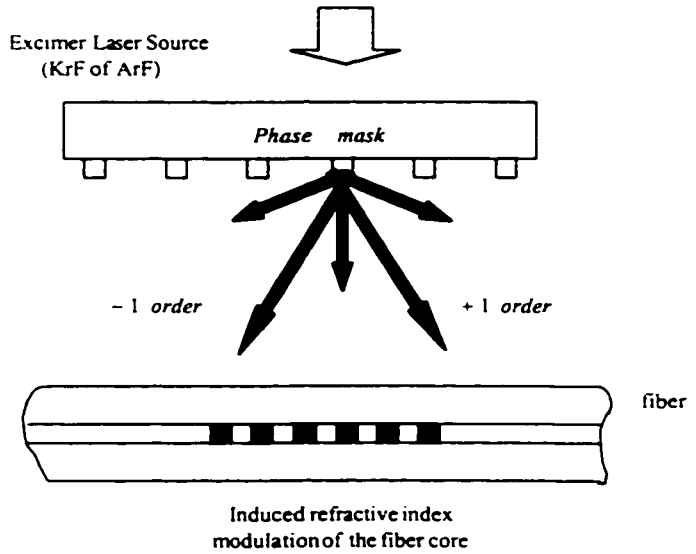

Figure 2-13. Fibre Bragg grating fabrication with phase mask technique.

The interference of the plus and minus first-order beams forms a fringe pattern in the near field. When a photosensitive fiber is placed in close proximity to the phase mask, exposure to the fringe pattern produces a permanent increase in the refractive index of the fiber, creating periodic modulation in the fiber core [51]. The period of the fringe pattern is half that of the mask, $\Lambda = \Lambda_{mask} / 2$, and the Bragg wavelength is then given by, $\lambda_B = 2n_{eff}\Lambda = n_{eff}\Lambda_{mask}$.

In comparison with the holographic technique, the phase mask technique simplifies the manufacture alignment procedures, reduces stability requirements on equipment, lowers coherence requirements on the UV laser beam, and permits the fabrication of several Bragg gratings in a single exposure thereby promising a low cost per unit Bragg grating. The repeatability is also high.

However, different phase masks are required for fabricating Bragg gratings at different resonant wavelengths. Some wavelength tuning is possible by applying tension to the fiber during the photo-imprinting process; the Bragg wavelength of the relaxed fiber shifts by about 2 nm. E-beam lithography minimum feature size imposes the limit on the lower Bragg wavelength, λ_B. Realistically, $\Lambda_{mask} < 550$ nm is not available. In practice, $\lambda_B < 830$ nm is not available.

Scanning phase mask technique

A variation of phase mask technique for writing Bragg gratings introduced by J. Martin *et al* [19], is shown in Figure 2-14.

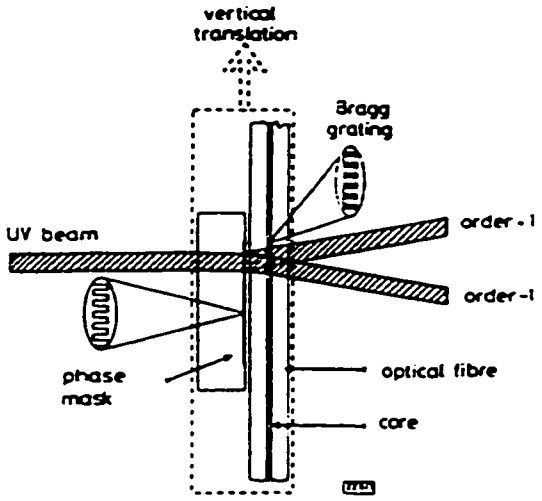

Figure 2-14. Scanning phase mask technique [19].

This method takes advantage of the insensitivity of the phase of the fringe pattern to the beam position. The idea is to keep the phase mask and the fiber together. The writing beam is tightly focussed on the fiber core and moved across mask and fiber assembly. The fringe contrast and periodicity in the fiber core are determined by the overlying mask. With this method, one can write gratings as long as the mask. Grating strength can be modified along the grating by controlling the writing intensity and one can control the grating length precisely.

2.3 Applications

Fiber Bragg gratings as an innovative technique have found broad applications and extensive potential market in fiber communications. These applications include rare-earth doped

fiber grating lasers [21], dispersion compensation [22], WDM Demultiplexers [23], WDM add/drop multiplexers [24], mode coupler [25], wavelength stabilization of laser diodes [26], hybrid fiber/semiconductor lasers [27], fiber amplifier gain control [28], grating based sensors [29], time delay for phased array radar [30], and nonlinear effect switches, [31] etc.

2.3.1 WDM Demultiplexers

In a WDM network, the signals at different wavelength channels are combined in a multiplexer, transmitted along the fiber link and then separated with a demultiplexer to direct each channel to its receiver. In the past, most WDM demultiplexers deployed technologies such as thin-film filters, bulk gratings, Fabry-Perot filters, and planar waveguides. These approaches suffered from performance limitations, especially for small channel spacing, e.g. 0.8 nm. FBGs appear to be best suited to meet the 0.8 nm channel spacing criteria.

Currently, two approaches have been employed for WDM demultiplexers using FBGs. The first approach uses optical circulators and gratings. Typically a circulator is a three-port device. A signal entering port 1 exits through port 2, while a signal entering port 2, leaves via port 3. Assume that, in a WDM configuration, multiple wavelengths, e.g. eight, enter port 1. If a Bragg grating with the Bragg wavelength corresponding to λ_3 is connected to port 2, then λ_3 will be reflected and exit through port 3, while the remaining wavelengths will leave through port 2, as shown in Figure 2-15. Two such devices placed back to back enable both drop and add functions.

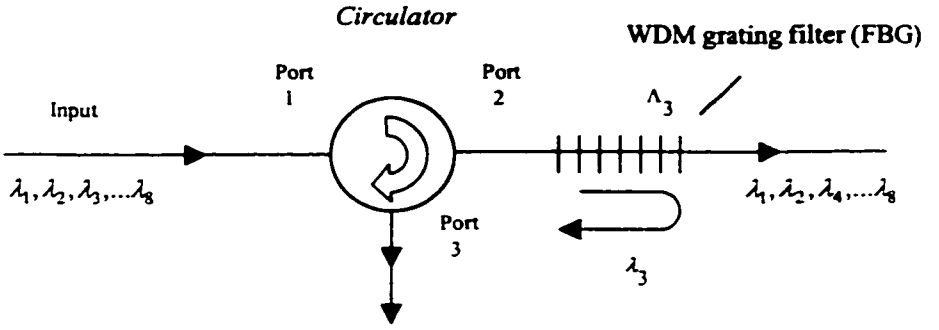

Figure 2-15. In a demultiplexer, FBG connected to port 2 reflected one wavelength of multiple-wavelength signal.

Low insertion loss (2 dB for add/drop channels, 3 dB thru channels) and high isolation of the drop and add channels (> 50 dB) was also achieved using the fiber-grating/optical circulator add/drop multiplexer [24].

The other approach incorporates FBGs and couplers in a Mach-Zehnder interferometer configuration, as shown in Figure 2-16. Two identical Bragg gratings are placed one in each arm of the device. Consider a stream of eight wavelengths ($\lambda_1, \lambda_2, \lambda_3, \ldots \lambda_8$) entering input port A. Assuming the Bragg grating's reflection wavelength is λ_3, light of λ_3 together with other wavelengths will be split equally between the two arms of the coupler. However, λ_3 will be reflected by the two identical gratings. At the coupling region, there is a coherent recombination. Then λ_3 exits at port B. The remaining wavelengths will continue to propagate, recombine, and exit through port D. Because of the symmetry of the device, wavelength λ_3 can be added at port C to come out with other wavelengths at port D.

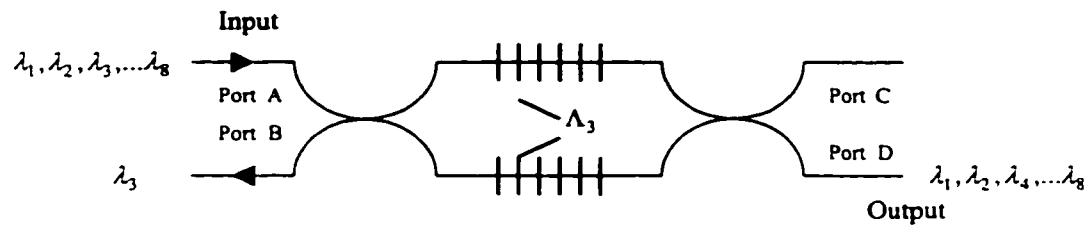

Figure 2-16. Identical Bragg gratings in a Mach-Zehnder interferometer configuration to direct one wavelength of multiple-wavelength signal.

2.3.2. **Dispersion compensation**

Chromatic dispersion in optical fiber causes different wavelength components of a data pulse to travel at different group velocities, broadening the signal pulse and increasing bit-error rates. As network data rates increase, chromatic dispersion in standard single-mode fiber becomes the main factor limiting performance. At a data rate of 2.5 Gbit/s, a signal can be transmitted without significant degradation for distances up to 1000 km. However, this distance drops sharply to 60 km at 10 Gbit/s and to a mere 15 km at 20 Gbit/s. In addition, a large portion of the worldwide installed fibers is optimized for transmission at 1310 nm. Such fiber exhibits high chromatic dispersion of about 17 ps/nm-km when used to transmit at the more commonly used telecom wavelength of 1550 nm.

Chirped FBGs are an attractive alternative to more conventional dispersion compensators [52-54]. FBGs are compact, passive, and commercially available at a reasonable cost. The basic principle of operation of a chirped fiber grating as a dispersion-compensating element is that different wavelength components of a broadened pulse are reflected at different locations along the grating, resulting in a differential group delay, as shown in Figure 2-17.

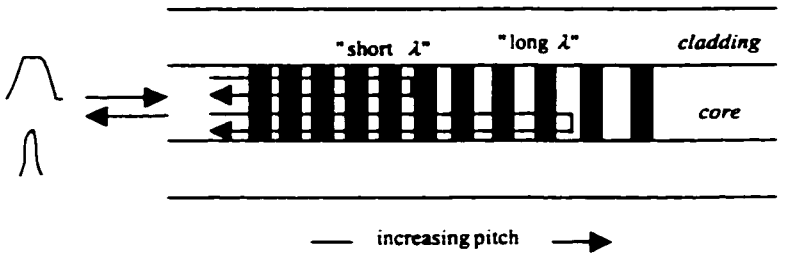

Figure 2-17. Schematic diagram of a chirped grating, illustrating dispersion compensation or pulse compression.

The maximum delay is proportional to the length of grating. Traditionally, one of the main limitations of this technique has been the narrow bandwidth associated with single gratings. It is, however, possible to cascade several gratings to arrive at a broadband device that can compensate for dispersion over moderate distances, as shown in Figure 2-18.

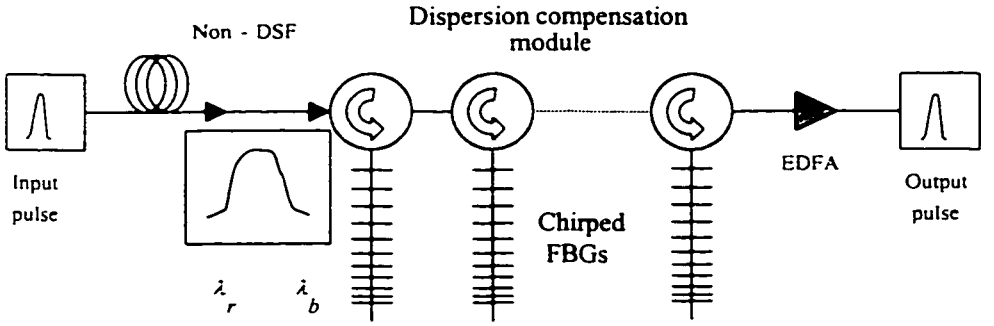

Figure 2-18. Chirped FBGs used to reshape optical pulses broadened by chromatic dispersion in fiber. Multiple gratings can be concatenated to achieve larger bandwidth.

2.3.3 Gain Equalizers

Erbium-doped fiber amplifiers (EDFAs) can amplify multiple wavelengths within a gain-bandwidth spectrum stretching from 1530 to 1560 nm. However, the gain is not uniform over the entire bandwidth. When an EDFA is used to amplify a multi-channel transmission, each channel experiences different gain. Concatenation of several amplifiers increases this nonunifromity, significantly reducing bandwidth. Eventually the gain discrepancy between the channels can become sufficiently large to be detrimental for WDM applications.

There are two basic approaches to flattening the gain spectrum. The first approach involves tailoring the material properties of the erbium doped fiber, either with the addition of extra dopants such as aluminum, or going to an altogether different host material, such as fluoride-based fiber [55] instead of silica based. However, with these methods the gain spectrum of EDFA is still not flat enough for an advanced DWDM system and there still remain other problems.

The second approach is to use gain-flattening filters. The principle of gain flattening is quite simple: filters are designed to approximate the inverse characteristics of the EDFA gain spectrum. Several technologies have been proposed in recent years, including microptic Mach-Zehnder filter, blazed Bragg gratings [46], acousto-optic tunable filters [56], and long period gratings [57].

Long period gratings appear to be the most promising candidates for gain flattening over other techniques due to the fact that they are passive, can be used in transmission and can be tailored to flatten the full 35 nm bandwidth. In addition, they exhibit low insertion loss, PDL and PMD, and are relatively easy to manufacture in a cost effective and consistent manner. A

typical EDFA gain spectrum is shown in Figure 2-19. Refer to Figure 2-6 for a typical long period grating spectrum.

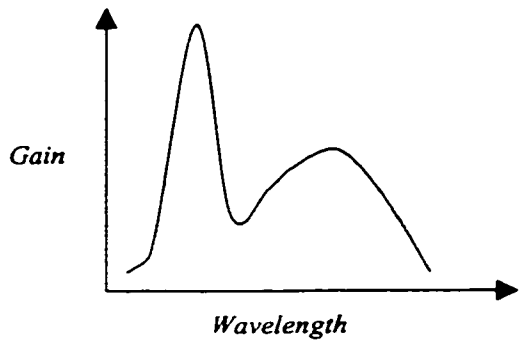

Figure 2-19. Typical EDFA gain spectrum.

Recently, long period grating filters were used to create a conventional Er fiber amplifier with > 40 nm of flat gain bandwidth [58].

Chapter 3

Representations of Polarized Light

The purpose of the chapter is to familiarize the readers with the concepts and mathematical representations of polarized light. Three calculational tools, i.e., the Jones calculus, the Mueller calculus, and the Poincare sphere are introduced to quantitatively describe the interaction of light with fiber-optic devices and to calculate the polarization properties, such as PMD and PDL of the devices. A model, the Principal States of Polarization (PSPs), used to describe the polarization dispersion for long fibers is also presented.

3.1 Jones Calculus

3.1.1 Jones Vector

The polarization of a lightwave signal is defined through electric fields. The electric field of a signal can be resolved into two orthogonal vector components. The state of polarization of a signal can be determined by the relative amplitude and phase of the E-field vector components. For a plane and monochromatic light wave travelling in the z-direction (fully polarized light wave), the complex exponential form of the electric field in column vector notation is given by:

$$\vec{E} = \begin{vmatrix} A_x e^{i\phi_x} \\ A_y e^{i\phi_y} \end{vmatrix} e^{i\omega t} = \vec{J} \cdot e^{i\omega t} \qquad (3\text{-}1)$$

where ω is the optical frequency, A_x, A_y and ϕ_x, ϕ_y are the amplitude and phase of the two orthogonal components, respectively, in rectangular coordinates, and $\vec{J}$ is known as the Jones vector given by:

$$\vec{\mathbf{J}} = \begin{vmatrix} A_x e^{i\phi_x} \\ A_y e^{i\phi_y} \end{vmatrix}. \qquad (3\text{-}2)$$

The intensity of a light signal, a more interesting quantity in experiments, is the sum of the squares of the amplitudes of the two electric field components, given by

$$\mathbf{I} = (\vec{\mathbf{J}} e^{i\omega t})(\vec{\mathbf{J}} e^{i\omega t})^* = \vec{\mathbf{J}} \cdot \vec{\mathbf{J}}^* = A_x^2 + A_y^2 \qquad (3\text{-}3)$$

Usually, the Jones vectors are denoted in their "standard normalized" forms. That is, the vectors are reduced to their simplest forms and have a magnitude of 1, satisfying the following condition

$$C^2 \vec{\mathbf{J}}^* \cdot \vec{\mathbf{J}} = 1, \qquad (3\text{-}4)$$

where C is a constant, and $\vec{\mathbf{J}}^*$ denotes complex conjugate of $\vec{\mathbf{J}}$.

For example, the standard Jones vectors for linear horizontal, vertical and 45 degrees polarized light take the form of $\begin{bmatrix} 1 \\ 0 \end{bmatrix}$, $\begin{bmatrix} 0 \\ 1 \end{bmatrix}$, and $\frac{\sqrt{2}}{2}\begin{bmatrix} 1 \\ 1 \end{bmatrix}$, respectively. For right- and left-handed circular polarization, the Jones vectors are $\frac{\sqrt{2}}{2}\begin{bmatrix} 1 \\ i \end{bmatrix}$, and $\frac{\sqrt{2}}{2}\begin{bmatrix} 1 \\ -i \end{bmatrix}$, respectively. Jones-vector representation is limited to the description of fully polarization light, i.e., light with a degree of polarization (DOP) of about 100 %) refer to section 3.2 for DOP definition).

3.1.2 **Jones Matrix**

The transmission properties of a two-port optical device can be described by a complex two-by-two Jones matrix [59]. The input light, represented by the Jones vector $\bar{\mathbf{J}}_{in}$, interacts with the optical device, represented by the Jones matrix **M**. The emerging light, represented by the Jones vector $\bar{\mathbf{J}}_{out}$ can then be determined by:

$$\bar{\mathbf{J}}_{out} = \mathbf{M} \cdot \bar{\mathbf{J}}_{in}. \tag{3-5}$$

For example, the Jones matrices of homogeneous horizontal, vertical, +45 and -45 degrees linear polarizers take the forms of $\begin{bmatrix} 1 & 0 \\ 0 & 0 \end{bmatrix}, \begin{bmatrix} 0 & 0 \\ 0 & 1 \end{bmatrix}, \frac{1}{2}\begin{bmatrix} 1 & 1 \\ 1 & 1 \end{bmatrix}$, and $\frac{1}{2}\begin{bmatrix} 1 & -1 \\ -1 & 1 \end{bmatrix}$.

The Jones matrix of an unknown optical device can be determined by measuring the three output Jones vectors responding to three input states of polarization, e.g., at 0, 45, and 90 degrees or any three distinct stimuli.

Assume that three Jones vectors, i.e., $\begin{bmatrix} X_1 \\ Y_1 \end{bmatrix}, \begin{bmatrix} X_2 \\ Y_2 \end{bmatrix}$, and $\begin{bmatrix} X_3 \\ Y_3 \end{bmatrix}$, are the measured output states of polarization corresponding to the three input linear polarization stimuli at 0, 45, and 90 degrees. Three complex ratios can be formed from these electric field components, $k_1 = X_1 / Y_1$, $k_2 = X_2 / Y_2$, $k_3 = X_3 / Y_3$, and $k_4 = (k_3 - k_2)/(k_1 - k_3)$. The Jones matrix is then given by:

$$\mathbf{M} = c\begin{bmatrix} k_1 k_4 & k_2 \\ k_4 & 1 \end{bmatrix}, \tag{3-6}$$

as shown in Figure 3-1. The matrix calculated here is related to the true Jones matrix by multiplying a complex constant c.

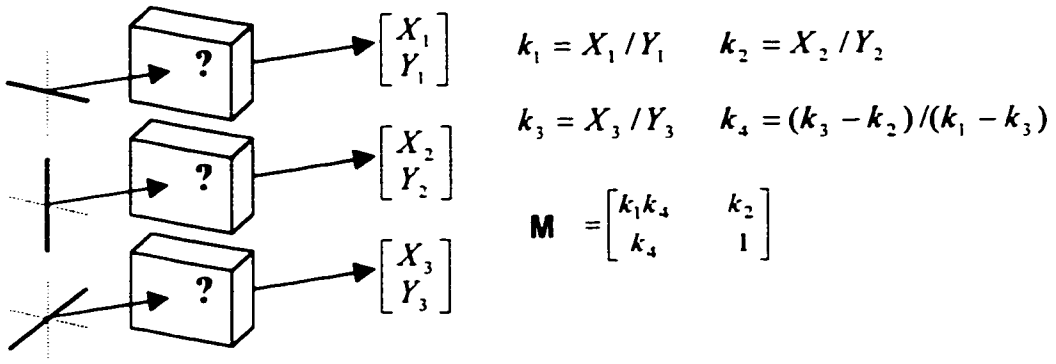

Figure 3-1. Measurement of the Jones matrix of an optical component.

The PMD and PDL values of an optical device can be calculated by determining the Jones matrices for a set of polarization states at adjacent frequencies/wavelengths, see Chapters 4 and 5 for details.

3.2 Stokes Parameters and Poincare Sphere

It is more convenient to measure the optical intensity/power instead of the electric field. In this case, the Stokes vector, a four-element array of optical intensity values in which the elements describe the optical intensity in particular reference polarization states, is widely used. Stokes vectors can also describe unpolarized or partially polarized light, whereas the Jones calculus cannot, since, by definition, light is described solely by two orthogonal and completely polarized components.

A common representation of the Stokes vector is given by [60]:

$$\vec{S} = \begin{bmatrix} S_0 \\ S_1 \\ S_2 \\ S_3 \end{bmatrix} = \{S_0 \quad S_1 \quad S_2 \quad S_3\} \tag{3-7}$$

where

S_0 = total optical intensity (polarized + unpolarized), (3-8a)

$S_1 = I_0 - I_{90}$ = difference in intensities between horizontal and vertical linearly polarized components, (3-8b)

$S_2 = I_{+45} - I_{-45}$ = difference in intensities between linearly polarized components oriented at $+45°$ and $-45°$, (3-8c)

$S_3 = I_{rcp} - I_{lcp}$ = difference in intensities between right and left circularly polarized components. (3-8d)

The last three Stokes parameters can be expressed in a rectangular coordinate system, shown in Figure 3-2. Here LH, LV, RC, and LC denote linear horizontal, linear vertical, right circular, and left circular polarizations, respectively. Linear polarized light at a particular angle is denoted as $L\pm\theta$. $s_1, s_2,$ and s_3 represent the normalized Stokes parameters, given by

$$s_1 = \frac{S_1}{S_0}, s_2 = \frac{S_2}{S_0}, s_3 = \frac{S_3}{S_0}. \tag{3-9}$$

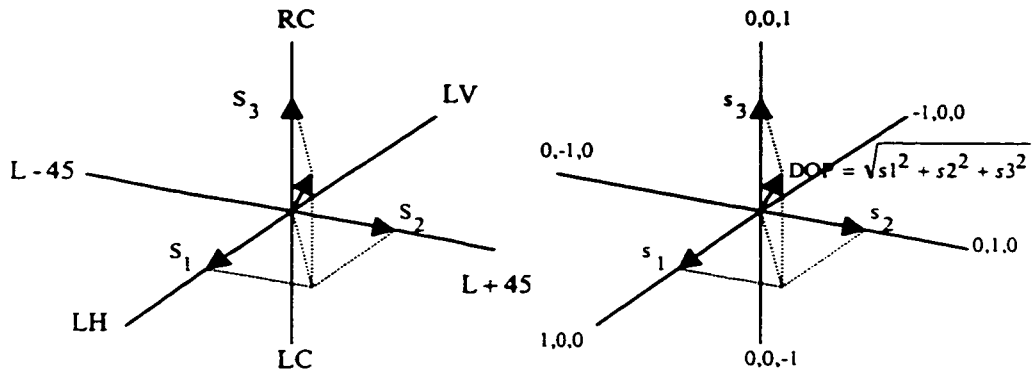

Figure 3-2. Orthogonal representation of (a) the Stokes parameters; (b) the normalized Stokes parameters.

The degree of polarization is given by the ratio of polarized light to total light:

$$\mathrm{DOP} = \frac{I_{\mathrm{polarized}}}{I_{\mathrm{polarized}} + I_{\mathrm{unpolarized}}} = \frac{\sqrt{S_1^2 + S_2^2 + S_3^2}}{S_0} = \sqrt{s_1{}^2 + s_2{}^2 + s_3{}^2}\,. \tag{3-10}$$

In the case of fully polarized light, DOP = 1, and Eqn (3-10) describes a sphere of unit radius.

If the light vector for completely polarized light propagating along the +z axis is expressed in terms of a rectangular coordinate system, as in Eqn. (3-1), then the relationship between the Stokes parameters and the electric field components can be expressed as:

$$S_0 = A_x^2 + A_y^2\,, \tag{3-11a}$$

$$S_1 = A_x^2 - A_y^2\,, \tag{3-11b}$$

$$S_2 = 2A_x A_y \cos\Delta\,, \tag{3-11c}$$

$$S_3 = 2A_x A_y \sin\Delta\,, \tag{3-11d}$$

where $\Delta = \phi_y - \phi_x$ is the phase difference between the E-field components, and $-180° < \Delta < +180°$.

Through a three-dimensional normalized Stokes vector $\{s_1\ s_2\ s_3\}$, the polarization state of any light wave can be uniquely represented by a point on the surface of a sphere on a rectangular coordinate system, called the Poincare sphere [61], as shown in Figure 3-3. Linear polarization states are located at the equatorial plane. Circular states are located at the poles, with intermediate elliptical states continuously distributed between the equator and the poles. It can be shown that orthogonal polarization states are located diametrically opposite one another on the sphere.

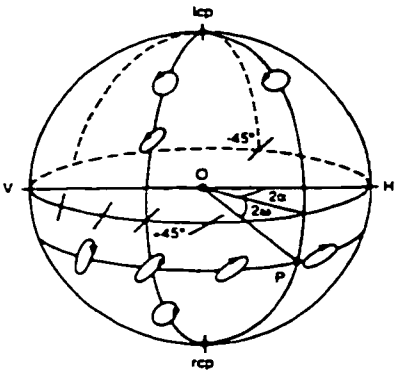

Figure 3-3. The Poincare sphere representation of polarized light [61].

The Stokes parameters, $s_0 \sim s_3$, can also be related to the complex electric field components by [61]:

$$s_0 = |E_x|^2 + |E_y|^2, \tag{3-12a}$$

$$s_1 = \frac{|E_x|^2 - |E_y|^2}{|E_x|^2 + |E_y|^2}, \tag{3-12b}$$

$$s_2 = \frac{E_x E_y^* + E_x^* E_y}{|E_x|^2 + |E_y|^2}, \tag{3-12c}$$

$$s_3 = \frac{i(E_x^* E_y - E_x E_y^*)}{|E_x|^2 + |E_y|^2}, \tag{3-12d}$$

where E_x, E_y are complex quantities denoting the amplitude and phase of the x and y directed components of the electric field.

3.3 **Mueller Calculus**

As with the Jones calculus, in the Mueller calculus, the interaction between a lightwave signal and an optical device can also be represented by the multiplication of a vector and a matrix. The difference is that the vector used to represent a lightwave signal is a four-element Stokes vector and it represents intensities rather than electric field components. Accordingly, the optical device is described by a four-by-four matrix.

The input light, represented by its Stokes vector $\vec{\mathbf{S}}_{in}$, interacts with an optical device, represented by a four-by-four matrix, called the Mueller matrix **M**. The emerging light is represented by its Stokes vector $\vec{\mathbf{S}}_{out}$, given as:

$$\vec{S}_{out} = \mathbf{M} \cdot \vec{S}_{in} = \begin{bmatrix} m_{11} & m_{12} & m_{13} & m_{14} \\ m_{21} & m_{22} & m_{23} & m_{24} \\ m_{31} & m_{32} & m_{33} & m_{34} \\ m_{41} & m_{42} & m_{43} & m_{44} \end{bmatrix} \cdot \vec{S}_{in}, \tag{3-13}$$

where **M** is the Mueller matrix of the optical device.

For example, the Mueller matrix of a horizontal and vertical linear polarizer will take the forms of $\frac{1}{2}\begin{bmatrix} 1 & 1 & 0 & 0 \\ 1 & 1 & 0 & 0 \\ 0 & 0 & 0 & 0 \\ 0 & 0 & 0 & 0 \end{bmatrix}$ and $\frac{1}{2}\begin{bmatrix} 1 & -1 & 0 & 0 \\ -1 & 1 & 0 & 0 \\ 0 & 0 & 0 & 0 \\ 0 & 0 & 0 & 0 \end{bmatrix}$, respectively.

The PDL of an optical device can be calculated by determining the first row of the Mueller matrix via measurements of the Stokes parameters at a set of polarization states, see Chapter 4 for details.

3.4 **Principal States of Polarization**

As we mentioned earlier, PMD originates from a phenomenon called birefringence. In short fiber or some fiber-optic devices, the birefringence distribution does not dependent on the position along the (fiber) length. Two orthogonal polarization modes exist and there is no energy exchange between them, so no mode coupling. In long fibers, the birefringence distribution is not uniform over the fiber length, but varies randomly from one point to another, resulting in energy exchange between the two electric field components/modes, called random or strong mode coupling, a phenomenon making PMD a function of wavelength and environmental conditions.

At a given wavelength, singlemode fiber or a fiber-optic component has pairs of input and output polarization states, or modes that represent the fastest and slowest propagation through

the device. Monochromatic light launched with a fixed input polarization state will propagate along the fiber/component and emerges with a different output polarization state. When the wavelength/frequency changes, the output state of polarization will also vary.

The question arising is: how is one to define the DGD in this case?

In 1986, C. D. Poole and R. E. Wagner introduced the concept of Principal State of Polarization (PSP), solving this problem [62]. The concept is based on the observation that for any linear optical transmission medium that has no PDL, there exist orthogonal input states of polarization (SOPs) for which the corresponding output SOPs are orthogonal and show no dependence on wavelength to first order. These states are called PSPs. They can be obtained by evaluating the eigenvectors of a system where the first-order dispersion is set to zero. In [62], under the assumption of no PDL, a complex transfer matrix $T(\omega)$ of a singlemode fiber or linear optical transmission medium can be represented by:

$$\mathbf{T}(\omega) = e^{\beta(\omega)} U(\omega), \tag{3-14}$$

where ω is the optical frequency, $\beta(\omega)$ is in general complex and $U(\omega)$ is a unitary matrix, taking the form:

$$U(\omega) = \begin{bmatrix} u_1(\omega) & u_2(\omega) \\ -u_2^*(\omega) & u_1^*(\omega) \end{bmatrix}, \quad \text{and} \quad |u_1|^2 + |u_2|^2 = 1. \tag{3-15}$$

A monochromatic optical field $\vec{\mathbf{E}}_{in}$, when transmitted by such fiber/fiber component, produces an output field $\vec{\mathbf{E}}_{out}$ given by:

$$\vec{\mathbf{E}}_{out} = \mathbf{T}(\omega)\vec{\mathbf{E}}_{in}. \tag{3-16}$$

The complex electric field components $\vec{\mathbf{E}}_{in,out}$ can be expressed in the form:

$$\vec{\mathbf{E}}_{in,out} = \begin{bmatrix} E^{x}_{in,out} \\ E^{y}_{in,out} \end{bmatrix} = \varepsilon_{in,out} e^{i\phi_{in,out}} \hat{\varepsilon}_{in,out} \tag{3-17}$$

where $\varepsilon_{in,out}$ and $\phi_{in,out}$ are the amplitude and phase of the fields and $\hat{\varepsilon}_{in,out}$ are complex unit vectors specifying the states of polarization.

Under the condition of fixed input state of polarization and a zero $\frac{d\hat{\varepsilon}_{out}}{d\omega}$ (no dispersion), the eigenvalues of the principal states of polarization can be obtained by solving:

$$[U^{-1}U' - i\kappa]\hat{\varepsilon}_{in} = 0, \tag{3-18}$$

leading to the two solutions of eigenvalues:

$$k = \pm\sqrt{\left|u'_1\right|^2 + \left|u'_2\right|^2}. \tag{3-19}$$

The corresponding eigenvectors are the principle states of polarization of the fiber or fiber-optic component. These vectors form an orthogonal pair and represent two orthogonal input

states whose corresponding output states are independent of frequency to first order. The propagation delay (group delay) between the two modes is then given by:

$$\Delta \tau = 2\sqrt{\left|u_1'\right|^2 + \left|u_2'\right|^2} \,. \tag{3-20}$$

The pair of orthogonal PSPs can be represented as a pair of diametrically opposite points on the Poincare sphere. When the frequency/wavelength of an arbitrary polarized input electric field varies, the point-end of Stokes vector corresponding to the output SOP will rotate on the Poincare sphere about the PSPs. From the rate of the rotation, the PMD can be determined, see Chapter 5 for details.

Chapter 4

PDL Measurement Techniques

In this chapter, the wavelength dependency of PDL in three types of fiber gratings commonly used in optical fiber communication systems is characterized. Chirped FBGs for dispersion compensation, WDM grating filters for add/drop multiplexing, and long period gratings for EDFAs' gain compensation are considered. Three measurement setups for implementing the Jones matrix method, the Mueller matrix method, and the polarization scanning method, have been implemented, and are discussed, compared and analyzed. Different calibration procedures were performed to account for the systems' PDL and the strong wavelength dependency of the setups. Typical measurement results and an uncertainty analysis are presented.

4.1 Definition of PDL

PDL is defined as the maximum change in the power transmitted by an optical component or device as the input state of polarization (SOP) is varied over all possible polarization states. The PDL contribution of individual components, when combined, can cause large power fluctuations in a system. This in turn may seriously affect the system's overall performance. In general, the total PDL of several concatenated components cannot be obtained by simply adding up the individual PDLs. Rather, individual PDLs should add as phasors; thus the total PDL is usually less than the sum of the individual PDLs. The sum of the individual PDLs, however, yields the worst-case system PDL.

There are two categories of PDL measurement techniques: deterministic and non-deterministic [63,64]. The deterministic techniques compute the PDL value from the device's

Jones or Mueller matrices, which are obtained via measurements of Stokes parameters for a set of prescribed input polarization states [65-67]. The non-deterministic techniques determine the PDL value by measuring the maximum polarization sensitivity of a device over all possible input polarization states. The PDL is then computed from:

$$PDL = 10 \log (T_{max}/T_{min}) \qquad (4\text{-}1)$$

where T_{max} and T_{min} denote the maximum and minimum power reflection or transmission through the device.

4.2 Theoretical Background

4.2.1 Polarization-Scanning Method

The polarization-scanning method (also called the power min/max method) is a non-deterministic measurement technique [1,2,68]. A polarization controller and a fast power meter are needed to determine the maximum and minimum changes in power transmission through the device over a large number of input polarization states. The polarization controller used must be able to convert a fixed input polarization state into all possible output polarization states, including linear, circular, and elliptical states. PDL wavelength response measurements are obtained by using a very stable tunable laser source. The power meter used must have low PDL. The measurement set-up used for characterizing optical components in reflection is shown in Figure 4-1. For measurements in transmission, the 3dB optical coupler is removed.

A power calibration procedure is required to remove the PDL contributions of the polarization controller and other optical components in the set-up. Accounting for the system

transmission variation, the wavelength dependent PDL of the device of test (DUT) is then determined according to Equation (4-1) as:

$$PDL(\lambda_i) = 10\log\left(\max\left(\frac{P_j^{DUT}(\lambda_i)}{P_j^{Cal.}(\lambda_i)}\right)\right) - 10\log\left(\min\left(\frac{P_j^{DUT}(\lambda_i)}{P_j^{Cal.}(\lambda_i)}\right)\right) \qquad (4\text{-}2)$$

where $\{\lambda_i\}$, i = 1, 2, ..., M, refer to wavelengths within the wavelength range of interest, $\{P_j\}$, j = 1, 2, ..., N, refer to the transmission/reflection power at a set of polarization states 1 to N. P^{Cal} and P^{DUT} denote the transmission/reflection power without the DUT (power calibration) and with the DUT, respectively. More details regarding calibration issues are given in Section 4.3.1.

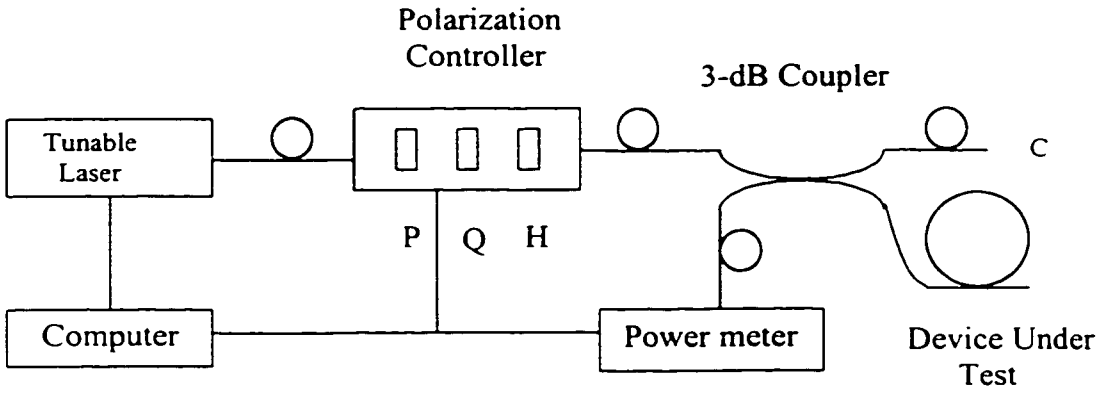

Figure 4-1. PDL measurement setup for characterizing a device in reflection using the polarization scanning method and the Mueller matrix method. The polarization controller comprises a polarizer (P), followed by a quarter-wave plate (Q) and a half-wave plate (H). The complementary output port C of the coupler is terminated to avoid back reflection.

The polarization scanning method can be time consuming even if an automated polarization controller and a fast power meter are used. This is especially true for wavelength dependent PDL measurements in broadband fiber optic components, since a large number of measurements must be obtained at each wavelength of interest to ensure measurement accuracy.

4.2.2 **Jones Matrix Method**

The theoretical background for the Jones matrix method has been discussed in chapter 3 and is also presented in [65]. The Jones matrix method measures the device's polarization response to three input states of polarization at a wavelength of interest. The PDL value of the DUT is then derived from these responses.

The measurement setup used for characterizing optical components in reflection is shown in Figure 4-2. For measurements in transmission, the 3dB optical coupler is removed. A polarization analyzer, having a polarization adjuster and a real-time (>1000 samples/s) polarimeter, is used to set three linear polarization states, measure the Stokes parameters for the three states, calculate the Jones matrix and derive the PDL value. Wavelength dependent measurements are accomplished by using a very stable tunable laser diode having a high resolution.

We assume that the Jones vector **x** represents the input electric field. In transmission, the fiber pigtails/cables interconnecting the DUT are represented by their Jones matrices **B** and **F**. In reflection, **B** and **F** represent the backward and forward Jones matrices of the 3dB optical coupler used shown in Figure 4-2, respectively. The DUT is represented by Jones matrix **A**. The output field through the optical coupler and the DUT can then be expressed as **BAFx**. The

Jones matrix of the coupler and DUT combined is **J = BAF**, which is obtained from the measured Stokes parameters for three linear input polarization states at 0, 60, and 120 degrees.

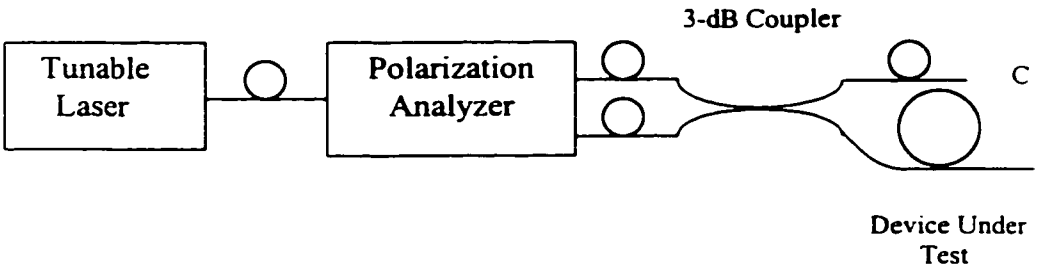

Figure 4-2. PDL measurement setup for characterizing a device in reflection using the Jones matrix method. The complementary output port C of the coupler is terminated to avoid back reflection.

The intensity of an input field **x** is proportional to the inner product $\langle \mathbf{x}, \mathbf{x} \rangle = \mathbf{x}^{*t}\mathbf{x}$, where $\mathbf{x}^{*t}$ denotes the conjugate transpose of vector **x**; thus the intensity is constant and normalized. The intensity of the output field is then proportional to the inner product $\langle \mathbf{Jx}, \mathbf{Jx} \rangle$. Measuring PDL involves finding the extrema of the inner product $\langle \mathbf{Jx}, \mathbf{Jx} \rangle$ over all input **x**. Since $\langle \mathbf{Jx}, \mathbf{Jx} \rangle = \langle \mathbf{J}^{*t}\mathbf{Jx}, \mathbf{x} \rangle$, the latter represents the field of values of a Hermitian matrix $\mathbf{J}^{*t}\mathbf{J}$, and according to [69], the extrema of the field of values of a Hermitian matrix **H** are given by the eigenvalues of **H**. Therefore the maximum and minimum reflected powers can be represented as $\lambda_i(\mathbf{J}^{*t}\mathbf{J}) = S_i^2(\mathbf{J})$ with i =1, 2, where λ_1 and λ_2 are the eigenvalues of $\mathbf{J}^{*t}\mathbf{J}$, and $S_i(\mathbf{J})$ are the singular values of matrix **J**. Thus:

$$\mathrm{PDL}_{meas.} = 10\log\frac{T_{\max}}{T_{\min}} = 10\log\left(\frac{\lambda_2(\mathbf{J}^{*t}\mathbf{J})}{\lambda_1(\mathbf{J}^{*t}\mathbf{J})}\right) = 10\log\left(\frac{S_2^2(\mathbf{J})}{S_1^2(\mathbf{J})}\right) = 10\log\left(\frac{S_2^2(\mathbf{BAF})}{S_1^2(\mathbf{BAF})}\right) \quad (4\text{-}3)$$

where $\mathbf{J}^{*t}$ denotes the complex conjugate transpose of matrix **J**, and $PDL_{meas.}$ denotes the measured PDL of DUT combined with the coupler.

In the case of the polarization-insensitive pigtails/cables used for the interconnection of the DUT in transmission, their Jones matrices **B** and **F** are unitary [65]. According to [69], the singular values of a square matrix are invariant under a unitary transformation. Then Equation (4-3) becomes:

$$PDL_{meas} = 10\log\left(\frac{S_2^2(\mathbf{BAF})}{s_1^2(\mathbf{BAF})}\right) = 10\log\left(\frac{S_2^2(\mathbf{A})}{S_1^2(\mathbf{A})}\right) = 10\log\left(\frac{\lambda_2(\mathbf{A}^{*t}\mathbf{A})}{\lambda_1(\mathbf{A}^{*t}\mathbf{A})}\right) = PDL_{DUT} \qquad (4\text{-}4)$$

where PDL_{DUT} denotes the PDL of the DUT. It can be seen from Equation (4-4) that the single-mode fibers/components interconnecting the DUT will not impair the measurement accuracy as long as they are polarization independent. This technique can then be used to characterize passive optical components even if the absolute phase delay in the fiber connections attached to the test device is drifting during the measurement.

The Jones matrix method is very fast; only two to three seconds are required for a PDL measurement at one wavelength. To remove the PDL contribution of the setup, a reference frame/power calibration procedure is needed. For a device used in reflection, the optical coupler may introduce measurement errors due to the slight polarization dependence of the coupler and the power fluctuation introduced by interference effects. More details regarding calibration issues are given in Section 4.3.1.

4.2.3 **Mueller Matrix Method**

The Mueller matrix method is based on exciting the DUT with four input polarization states (linear horizontal, linear vertical, linear at +45 degrees and circular) and measuring the optical power transmission at these four states only [66,67]. The incident polarized light, characterized by the Stokes vector $\bar{\mathbf{S}}_{in}$, interacts with the optical component, which is represented by a 4x4 Mueller matrix M. The emerging light, characterized by the Stokes vector $\bar{\mathbf{S}}_{out}$, can then be expressed as:

$$\bar{\mathbf{S}}_{out} = \mathbf{M} \cdot \bar{\mathbf{S}}_{in} = \begin{bmatrix} m_{11} & m_{12} & m_{13} & m_{14} \\ m_{21} & m_{22} & m_{23} & m_{24} \\ m_{31} & m_{32} & m_{33} & m_{34} \\ m_{41} & m_{42} & m_{43} & m_{44} \end{bmatrix} \begin{bmatrix} S_0 \\ S_1 \\ S_2 \\ S_3 \end{bmatrix}_{in} \tag{4-5}$$

where S_0, S_1, S_2, and S_3 are defined in Eqns. (3-8a) to (3-8d).

Only the matrix elements of the first row of the Mueller matrix, m_{11}, m_{12}, m_{13} and m_{14}, are used for PDL calculation because $S_{0_{out}}$ represents the total output power:

$$S_{0_{out}} = m_{11}S_{0_{in}} + m_{12}S_{1in} + m_{13}S_{2_{in}} + m_{14}S_{3_{in}}. \tag{4-6}$$

These four elements can be determined, at each wavelength, by measuring the optical power at the input of the DUT (power calibration) and the corresponding optical powers at the output of the DUT for the four polarization states at 0, +45, 90 degrees linear and circular. Then they can be calculated as:

$$m_{11}(\lambda_i) = \frac{1}{2}\left(\frac{P_1^{DUT}(\lambda_i)}{P_1^{Cal.}(\lambda_i)} + \frac{P_2^{DUT}(\lambda_i)}{P_2^{Cal.}(\lambda_i)}\right) \tag{4-7a}$$

$$m_{12}(\lambda_i) = \frac{1}{2}\left(\frac{P_1^{DUT}(\lambda_i)}{P_1^{Cal.}(\lambda_i)} - \frac{P_2^{DUT}(\lambda_i)}{P_2^{Cal.}(\lambda_i)}\right) \tag{4-7b}$$

$$m_{13}(\lambda_i) = \frac{P_3^{DUT}(\lambda_i)}{P_3^{Cal.}(\lambda_i)} - m_{11}(\lambda_i) \tag{4-7c}$$

$$m_{14}(\lambda_i) = \frac{P_4^{DUT}(\lambda_i)}{P_4^{Cal.}(\lambda_i)} - m_{11}(\lambda_i) \tag{4-7d}$$

where $\{\lambda_i\}$, i = 1, 2, ..., M, refer to wavelengths within the wavelength range of interest and $\{P_j^{Cal}, P_j^{DUT}\}$, j = 1, 2, 3, 4, denote the optical power without the DUT and with the DUT, respectively, at the four polarization states. This power calibration reduces the PDL contribution from the setup.

The maximum and minimum power transmission are calculated as:

$$T_{max}(\lambda_i) = m_{11}(\lambda_i) + \sqrt{m_{12}^2(\lambda_i) + m_{13}^2(\lambda_i) + m_{14}^2(\lambda_i)} \tag{4-8}$$

$$T_{min}(\lambda_i) = m_{11}(\lambda_i) - \sqrt{m_{12}^2(\lambda_i) + m_{13}^2(\lambda_i) + m_{14}^2(\lambda_i)} \tag{4-9}$$

and the PDL of the DUT at each wavelength (λ_i) is obtained from Equation (4-1).

The measurement setup for the Mueller matrix method for characterizing optical components in reflection is shown in Figure 4-1 <p48>. For measurements in transmission, the 3-dB optical coupler is removed. The key instrument in this setup is the polarization controller, which is

comprised of a polarizer, a quarter-wave plate and a half-wave plate. The quarter and half-wave plates are used to synthesize the four polarization states, while the polarizer is used to ensure that the input signal is polarized along a fixed orientation. Before the measurements can begin, the polarizer should be aligned with the incident polarized signal to achieve maximum transmission through the polarization controller. Wavelength dependent measurements are obtained using a very stable tunable laser diode having a high resolution.

Similar to the Jones matrix method, the Mueller matrix method is also fast, requiring only a few seconds per power measurement at the wavelength of interest. For more details on calibration procedures refer to Section 4.3.1.

4.3 Experimental Results and Discussion

As described in the previous section, we have implemented the polarization-scanning method, the Jones matrix method, and the Mueller matrix method to measure the wavelength dependent PDL of passive optical components used in reflection or transmission as shown in Figures 4-1 and 4-2. A stable wavelength tunable laser diode TUNICS-PRI from Photonetics, a JDSfitel polarization controller, a HP8509B polarization analyzer, and a HP8153 Lightwave multimeter with HP81533B Optical Head were used for the measurements. Optical connectors were used to connect the DUT to the set-up. The polarization controller yields an output signal that has the desired polarization with a high degree of polarization.

The fiber cables/pigtails and fiber-optic components in the setups must not be moved during the measurements to avoid changes in the polarization state passing through these components. The wavelength was scanned over the wavelength range of interest using an appropriate step, which depends on the bandwidth of the device. Narrowband, single-channel

fiber Bragg gratings for dispersion compensation and WDM grating filters for wavelength add/drop multiplexing have been characterized using a wavelength step of 0.01 nm, while broadband devices such as long period gratings for gain flattening of EDFAs have been characterized using a 0.2 nm step size.

4.3.1 **Calibration Issues**

Different calibration procedures are necessary to account for the system PDL and these depend on the measurement technique we used and on whether we are measuring narrowband or broadband components.

4.3.1.1 **Power Calibration**

For measurements using the polarization-scanning method, a power calibration procedure is required to remove the PDL contributions of the polarization controller and other optical components in the set-up. We calibrate the set-up for a large number of input polarization states by measuring the transmission variation through the whole system without the DUT versus polarization at each wavelength of interest. We then measure the transmission variation through the whole system with the DUT for the same polarization states at the same wavelengths. A polarization analyzer was used to monitor the input polarization states to ensure a quasi-random rotation pattern to uniformly cover the whole Poincaré sphere after a certain scanning time. Subtracting the system transmission variation, we can obtain the wavelength dependent PDL of DUT using Equation (4-2).

For the Jones matrix method, a power calibration is needed to account for the polarization sensitivity of the polarization analyzer. This can be accomplished by applying the internal

calibration procedure that is provided with the HP8509B polarization analyzer. First, the system transmission variation is measured with a short polarization insensitive fiber cable and a three-point reference frame is applied at each wavelength of interest. This is followed by the power transmission measurements with the DUT at the same wavelengths.

For measurements using the Mueller matrix method, a two-step procedure consisting of a power calibration followed by a power measurement is performed to obtain the PDL value of the DUT. First, the optical power is measured without the DUT at the four polarization states to account for the power variations caused by the polarization controller (the wave plates) from one polarization state to another. Next, the optical power is measured with the DUT for the same polarization states. The polarization analyzer was used to display the input polarization states to the DUT to ensure that the four required polarization states were accordingly set by adjusting the quarter and half-wave plates of the polarization controller. The PDL of the DUT at each wavelength is then be calculated using Equations (4-8), (4-9) and (4-1).

Power calibration should be undertaken before a series of measurements. With just one calibration several devices can be measured one by one.

4.3.1.2 **Wavelength Dependent Calibration**

Due to the strong wavelength dependence of the polarization components in the instrumentation, a wavelength dependent calibration must be performed over the bandwidth of interest. The interval of wavelength calibration, typically a few nanometers, depends on the accuracy required.

In the case of narrowband devices, such as single-channel dispersion compensation gratings or WDM grating filters (3-dB bandwidth of about 0.8 nm), the wavelength dependence of the

system components can be ignored. In the case of broadband devices, such as long period gratings (bandwidth of about 30 nm), however, the strong wavelength dependence of the system components must be compensated.

For measurements of broadband fiber devices using the Jones matrix method, a wavelength dependent calibration was performed to reduce the wavelength dependence in the internal reference frame of the HP8509B polarization analyzer. In order to acquire an accuracy of 0.02 dB or 0.03 dB in the reference frame, the calibration should be carried out at an interval of 3 or 5 nanometers, respectively. A three-point reference frame is taken at the central wavelength of one calibration interval, then the DUT is measured over this interval with the chosen wavelength step. This calibration-measurement procedure is repeated within the wavelength range of interest.

For measurements using the Mueller matrix method, a wavelength-dependent calibration was performed to account for the wavelength dependence in the wave plates of the polarization controller. A wavelength-dependent setting of the half and quarter wave plates in the polarization controller should be undertaken every 3 to 5 nanometers. Before measurements, the angles of the polarizer (P), the quarter wave plate (Q) and half wave plate (H) corresponding to the four required polarization states have to be re-adjusted at an interval of 3 to 5 nm. A table with these angular settings is then filled out. The required polarization states are monitored by the HP polarization analyzer, and in each measurement, the computer looks up the table and asks the polarization controller to set its polarizer and waveplates accordingly.

The wavelength dependent calibration should be carried out each time before any measurements are taken.

4.3.1.3 **Measurements In Reflection**

To measure a device used in reflection, such as dispersion compensation gratings and WDM grating filters, an auxiliary optical component, a 3-dB coupler or a circulator, must be added to the measurement setup, which increases the uncertainty of the measurements. The calibrations in reflection for the Mueller matrix method and polarization-scanning method are performed using an optical coupler and/or a gold-coated mirror, as shown in Figure 4-3.

There are two calibration schemes for measurements in reflection. In Scheme 1, the experimental setup is calibrated at port D. The DUT is then connected to port D, and the reflected power measured at port C. Here, the measured PDL is the PDL of the DUT combined with coupler (D → C). In Scheme 2, the experimental setups are calibrated at Port C with a gold-coated mirror connected to port D. In this case, the PDL of the gold-coated mirror is introduced into the measurement results. Since the 3-dB coupler and the gold-coated mirror used have PDLs below 0.02 dB, the difference between the two schemes is very small, within an accuracy of 0.02 to 0.03 dB.

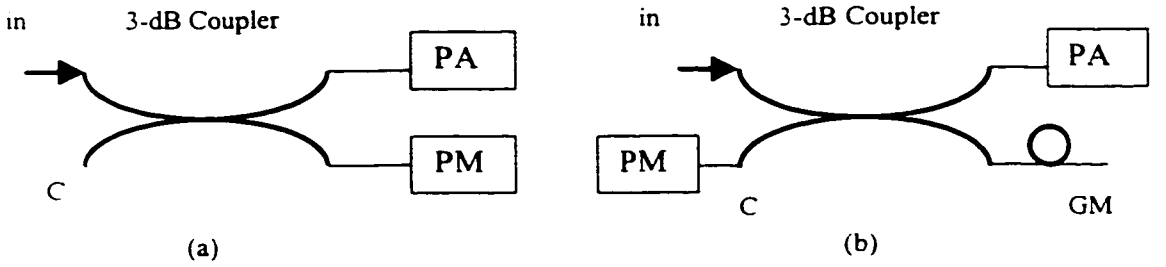

Figure 4-3. Calibrations in reflection with a 3-dB optical coupler and/or a gold-coated mirror for the Mueller matrix method and polarization-scanning method. (a) Scheme 1: calibration at port D of the coupler. The complementary output port C of the coupler is terminated to avoid back reflection. (b) Scheme 2: calibration at port C with a gold-coated mirror connected at port D of the coupler. PA: polarization analyzer. PM: power meter. GM: gold-coated mirror.

For the Jones matrix method in reflection, the calibration schemes are similar except that the power meter is replaced by the polarization analyzer.

4.3.2 **Measurement Results**

The wavelength dependence of the system PDL for our three experimental setups when used in transmission over a broad bandwidth is shown in Figure 4-4. Only the transmission mode is measured because the gratings used in reflection are narrowband. The wavelength-dependent calibration procedure was repeated every 3 nm over a bandwidth of about 30 nm to obtain an accuracy of 0.02 dB in the reference frame. It can be seen from this figure that the system PDL in these setups for the Jones matrix method and the Mueller matrix method are relatively low, about 0.017 dB and about 0.025 dB on average, respectively. For the polarization-scanning method, the system PDL of our setup is much higher, about 0.12 dB, due to the insertion loss variation with rotation of the polarization controller used.

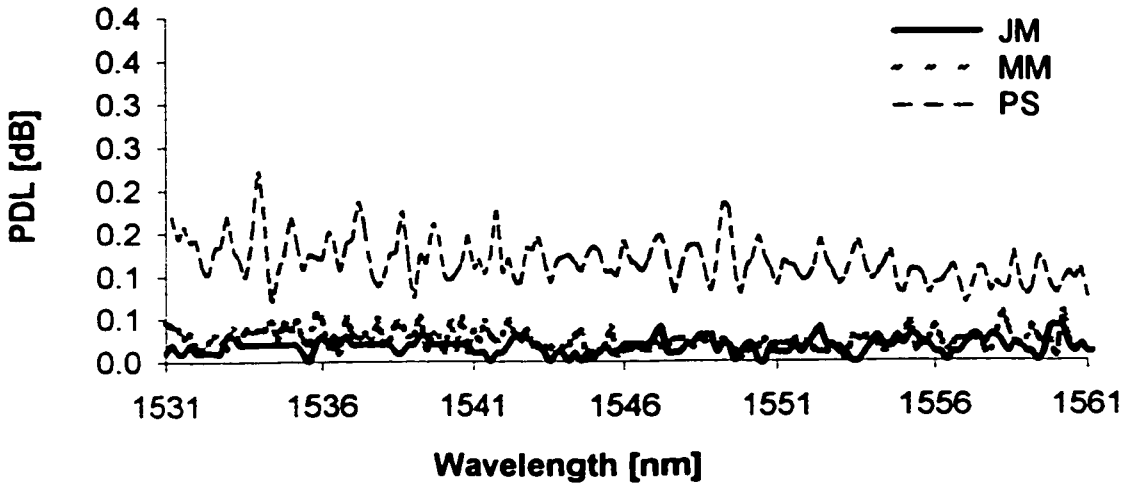

Figure 4-4. Measurement results for our setups. The wavelength dependent PDL is measured using the Jones matrix method (JM), the Mueller matrix method (MM), and the polarization scanning method (PS).

The wavelength dependent PDL of a chirped fiber Bragg grating, used in reflection as a dispersion compensator, and a grating filter, used in reflection for WDM add/drop multiplexing, have been measured using these setups. The results are shown in Figures 4-5 and 4-6 respectively. The measured reflection responses are also shown for reference. It can be seen that the measured PDL is very high outside the 3-dB reflection bandwidth due to the lower power level and the large ripples in the reflection response. The typical PDL values within the 3-dB bandwidth of the dispersion compensation gratings are low, varying from 0.01dB to 0.14dB. That is why only the Jones matrix and Mueller matrix methods were used for characterizing the grating. Due to the high system PDL, the experimental setup for the polarization-scanning method could not be used (see Figure 4-4).

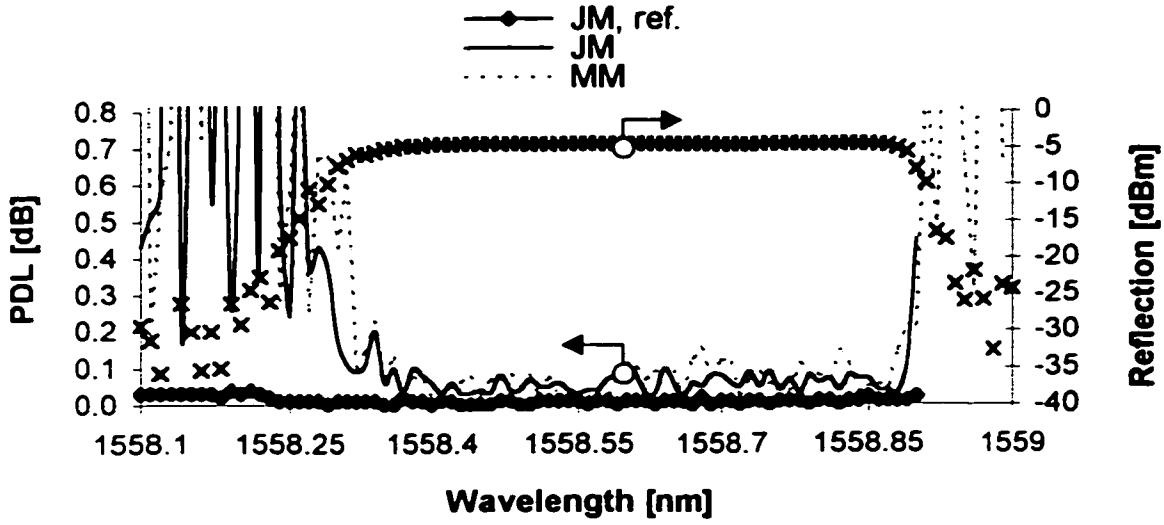

Figure 4-5. Measurement results for a dispersion compensation grating. The wavelength dependant PDL is measured using the Jones matrix method (JM) and the Mueller matrix method (MM). The system PDL (JM, ref) and the reflection response are shown for reference.

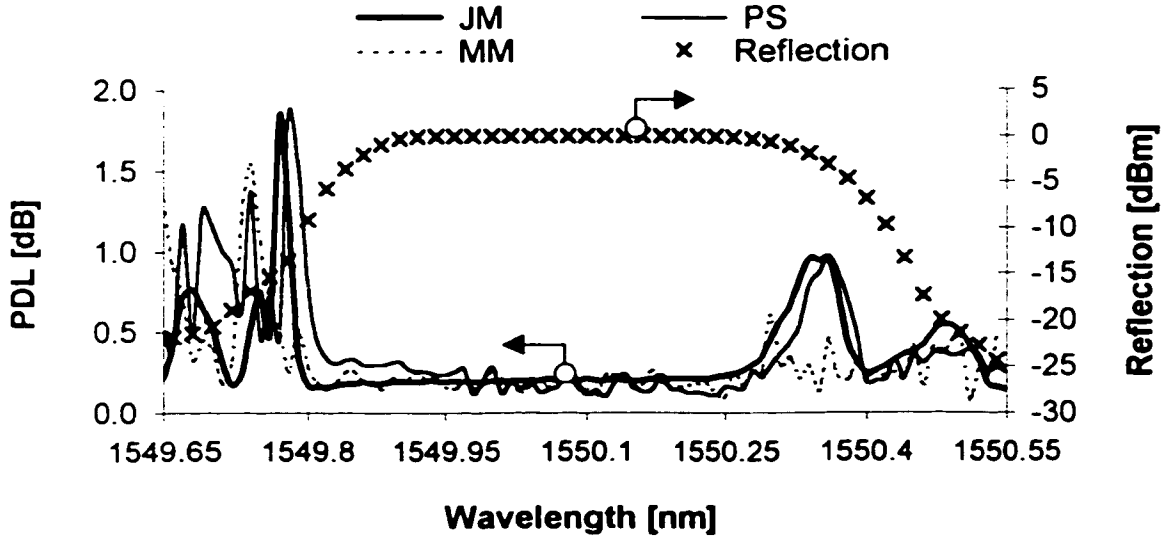

Figure 4-6. Measurement results for a WDM grating filter. The wavelength dependent PDL is measured using the Jones matrix method (JM), the Mueller matrix method (MM) and the polarization scanning method (PS). The reflection response is shown for reference.

The typical PDL values of the WDM grating filter are higher within its 3-dB bandwidth, varying from 0.15 to 0.25dB. Peaks in measured PDL appear slightly shifted on the wavelength scale due to the tuning repeatability of the laser source, which is ±0.005 nm. The 3-dB bandwidths of the dispersion compensation grating and the WDM grating are small, about 0.6 nm and 0.8 nm respectively, and in this case the wavelength dependence of the setup is negligible. The wavelength calibration of the setups in reflection for the Jones matrix and the Mueller matrix methods were performed at the center wavelength only according to Figure 4-3 (a) Scheme 1.

The wavelength dependent PDL of a long period grating used in transmission for EDFA gain flattening has been obtained using the three setups shown in Figures 4-1 and 4-2. In this case the 3-dB fiber optic coupler was removed and the device connected directly either to the polarization controller and power meter, or to the optical input and output ports of the polarization analyzer. Figure 4-7 shows the measured wavelength dependent PDL and transmission response for the long period grating. As observed from Figure 4-7, this grating has a smooth spectral response. The measurements were performed using a wavelength step of 0.2 nm and no ripples were observed. A slight shift in the minimum PDL compared to that in the transmission response can be observed due to the tuning repeatability of the laser source, which is ±0.005 nm. For the measured long period gratings with a 3-dB bandwidth of about 30 nm, the calibration procedure was repeated every 5 nm, yielding an accuracy of ±0.03 dB in the reference frame.

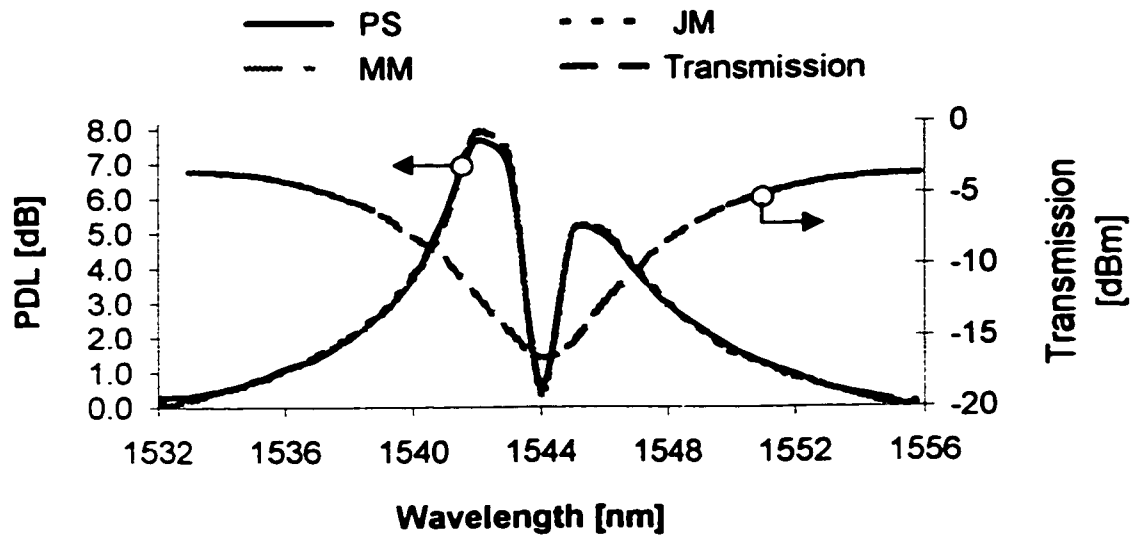

Figure 4-7. Measurement results for a long period grating. The wavelength dependant PDL is measured using the Jones matrix (JM) method, the Mueller matrix (MM) method and the polarization scanning method (PS). The transmission response is shown for reference.

The range of PDL values generated by the three components characterized in this study is large and as seen from Figures 4-5, 4-6 and 4-7, the dynamic ranges associated with these experimental setups are also quite large. Good agreement between measurements obtained using the different techniques is also found.

4.4 Uncertainty Analysis

Power fluctuations in the setups due to fluctuations in the output power of the laser and the rotation of the polarization plates in the polarization controller during measurements are the major sources of PDL errors and must be taken into account. Thermal instabilities may also affect the accuracy of the measured PDL and increase the uncertainty in the measurement

results. At least one hour of warm-up time is needed for most instruments to achieve thermal stabilization. Fiber cables and fiber-optic components in the measurement setups must not be moved during a measurement to ensure that the polarization transfer function of the components remains unchanged. Usually a few minutes waiting time is sufficient for the fiber components to stabilize after they are disturbed. Connector pairs cause reflections at the connector interface and increase the uncertainty in the measured PDL. Proper care of the connectors and fusion spliced connections can reduce the PDL uncertainty. To measure a device used in reflection, another optical component, a 3-dB coupler or a circulator must be added to the measurement setup, which increases the uncertainty of the measurements. The individual elements in a PDL measurement setup randomly contribute to the measurement uncertainty. The total PDL uncertainty is the root sum squared of the individual PDL uncertainties in the setup. In the worst scenario, the total PDL uncertainty is the sum of the systematic uncertainties and the measurement uncertainties.

4.4.1 **Polarization-Scanning Method**

The major sources of uncertainty in the polarization scanning method originate from the finite scanning time for the polarization controller and the systematic uncertainty. The main contributors to the systematic uncertainty include the PDL and linearity of the power meter, fluctuations in the laser's output power and power fluctuations due to the polarization controller when scanned in a quasi-random rotation pattern.

The individual uncertainties in our setup are: <0.01 dB laser output power stability over one hour, 0.1 dB insertion loss variation with rotation for the polarization controller, 0.005 dB power sensor PDL, 0.04 dB power sensor linearity, 0.02 dB connector pair PDL, and 0.02 dB optical

coupler (used in reflection) PDL. The total system uncertainty is the root sum squared of the individual uncertainties and is 0.11 dB when a connector pair is used or 0.108 dB if connections are fusion spliced in transmission. In reflection, the 0.02 dB PDL of the optical coupler has to be added. In the worst case, the total system uncertainty is the sum of the individual uncertainties and is 0.175 dB when a connector pair is used or 0.155 dB if connections are fusion spliced in transmission. The PDL of an optical component cannot be measured if the component has a PDL value less than the relevant worst-case uncertainty.

Ideally, the polarization-scanning method should be performed over all possible polarization states. In practice, this cannot be the case and an error is introduced due to the finite set of polarization states generated. To obtain an accurate PDL measurement, a certain scanning time is needed, which is related to the maximum allowable longitudinal angular step δ and latitudinal angular step γ on the Poincaré sphere, as shown in Figure 4-8.

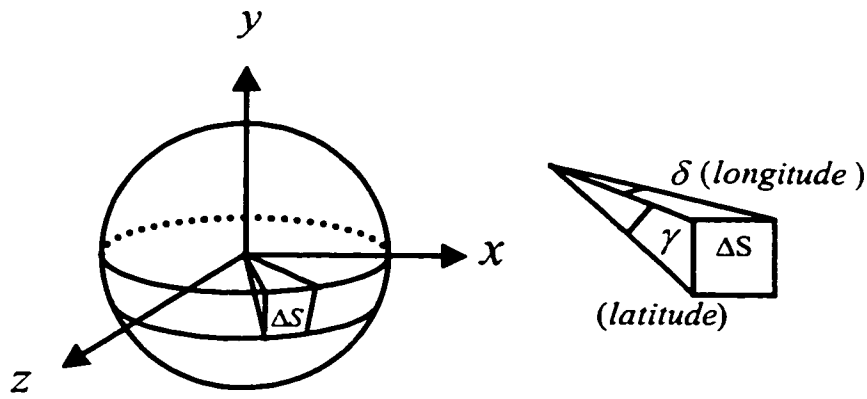

Figure 4-8. Poincaré Sphere of polarization states and angular steps.

The longitudinal angular step δ determines the number of measurement samples M to be taken for one circle on the Poincaré sphere: $\delta = 2\pi/M$. The number of measurement circles N is

related to the latitudinal angular step γ via: $\gamma = \pi/N$. Assuming that the whole sphere is discretized in steps of δ and γ, the measurement uncertainty ε is then given by:

$$\varepsilon = \frac{\Delta S}{S_{sphere}} \approx \frac{\delta\gamma}{4\pi} \tag{4-10}$$

where ΔS and S_{sphere} denote the surface of uncovered area between two steps and the surface of the Poincaré sphere respectively. The corresponding total scanning time T_{total} required to cover the whole surface of the Poincaré sphere is given by:

$$T_{total} = NM\Delta t = \frac{\pi\Delta t}{2\varepsilon} \tag{4-11}$$

where Δt is the time required to obtain one measurement. If we choose $\delta=\gamma$, then from Equations (4-10) and (4-11) we see that the measurement uncertainty is proportional to the square of the angular step on the Poincaré sphere and inversely proportional to the total scanning time. The larger the angular step, the larger the measurement uncertainty and the shorter the scanning time.

For instance, to achieve a 0.5% measurement uncertainty, an angular step of 14.4 degrees is allowed. For a power meter averaging time of Δt = 20 ms, 6.3 seconds total scanning time is needed for one PDL measurement.

The minimum angular steps δ_{min} and γ_{min} are given by the product of the polarization controller's angular velocity of rotation v and the averaging time of the power meter Δt : $\delta_{min} = \gamma_{min} = v\Delta t$. The minimum measurement uncertainty is then given by:

$$\varepsilon_{min} = \frac{\delta_{min}\gamma_{min}}{4\pi} = \frac{(v\Delta t)^2}{4\pi} . \qquad (4\text{-}12)$$

In our measurement setup, v = 36 deg/s for the polarization controller and Δt = 20 ms for the power meter which yields δ_{min} = 0.72 degrees. The corresponding minimum measurement uncertainty is 0.008%. To achieve this level of uncertainty, 6.5 minutes total scanning time is needed for one PDL measurement at one wavelength.

4.4.2 **Mueller Matrix Method**

The major sources of uncertainty in the Mueller matrix method originate from the system uncertainty and the angular accuracy of the polarization controller and polarization analyzer. The main contributors to the system uncertainty include the power meter's PDL (0.005 dB), fluctuations in the laser's output power (0.01 dB over one hour) and power fluctuations in the light passing through the polarization controller. In addition, the larger of the angular uncertainty of the polarization controller or the angular uncertainty of the polarization analyzer must be taken into account. Here the polarization analyzer was used to monitor the input polarization states to the DUT as described in Section 4.3.1. The angular uncertainty is 0.25 degrees for the polarization controller and 1 degrees for the polarization analyzer.

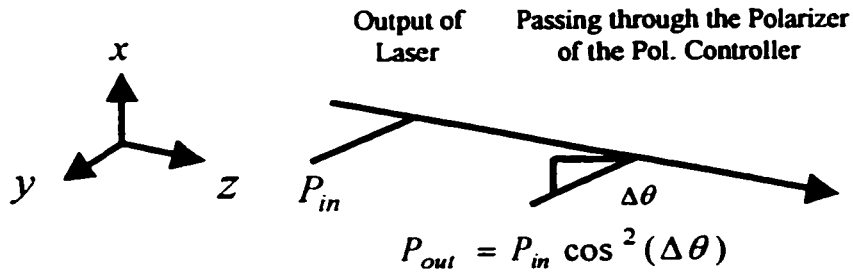

Figure 4-9. Power fluctuations induced by the angular uncertainties.

As shown in Figure 4-9, the output power of the polarization controller is related to the incident power and the angle Δθ via:

$$P_{out} = P_{in} \cos^2(\Delta\theta) \tag{4-13}$$

where Δθ (≠0) denotes the angle between the axes of the input and output of the polarizer in the polarization controller or the minimum angle step of the polarization analyzer, whichever is larger, and P_{in} and P_{out} denote the input and output powers into and out of the polarizer respectively. Taking variations in Equation (4-13):

$$\delta P_{out} = \delta P_{in} \cos^2(\Delta\theta) + P_{in} 2\cos(\Delta\theta)\{-\sin(\Delta\theta)\}\delta\Delta\theta \tag{4-14}$$

where δΔθ denotes the angle uncertainty in axis alignment between input and output light passing through the polarization controller.

The relative error in the output power is then obtained by dividing Eq. (4-14) by :

(4-15)

The axes should be aligned to give maximum throughput. Since $\Delta\theta$ and $\delta\Delta\theta$ are very small, we can assume that $\Delta\theta \approx \delta\Delta\theta$. Then Equation (4-15) can be approximated as:

(4-15)

In our case, $\Delta\theta = \delta\Delta\theta = 1$ degree, which yields = 0.137% in output power fluctuation or a 0.012 dB PDL uncertainty.

The total system uncertainty is the root sum squared of the individual uncertainties mentioned above, and is 0.026 dB with a connector pair or 0.016 dB when connections are fusion spliced in transmission, 0.036 dB with a connector pair or 0.03 dB when connections are fusion spliced in reflection. In the worst case, the total system uncertainty is the sum of the individual uncertainties, and is 0.047 dB with a connector pair or 0.027 dB when connections are fusion spliced in transmission, and 0.67 dB with a connector pair or 0.47 dB when connections are fusion spliced in reflection.

4.4.3 **Jones Matrix Method**

The major sources of error in the Jones matrix method originate from the power drift of the laser source and the internal PDL of the polarization analyzer. The PDL of the polarization analyzer and the system can be reduced by applying power and wavelength calibrations.

The individual uncertainties in the setup shown in Figure 4-2 include a 0.01 dB laser source stability over one hour, a 0.1 dB polarization dependence of the polarization analyzer, a 0.02 dB connector pair PDL, and a 0.02 dB optical coupler PDL when the set-ups used in reflection. The total system uncertainty is the root sum squared of the individual uncertainties mentioned above, which is 0.102 dB with a connector pair and 0.1 dB when connections are fusion spliced in transmission, and 0.104 dB with a connector pair and 0.1 dB when connections are fusion spliced in reflection. This is the minimum PDL for this specific measurement setup. With a three-point reference frame, the internal PDL of the polarization analyzer is reduced to 0.02~0.03 dB.

For a measurement in reflection, another system error comes from the method assumption that fiber cables and pigtails used for interconnection have no PDL, and thereby their Jones matrices are unitary. In reflection, a fiber-optic coupler with small PDL (in both directions) is used. The measured PDL is the combined PDL of DUT and the coupler. The small PDL of the 3-dB optical coupler used in reflection makes $\mathbf{B}$ and $\mathbf{F}$ non-unitary, which means, $PDL_{meas} \neq PDL_{DUT}$. Here $\mathbf{B}$ and $\mathbf{F}$ represent the Jones matrices of the 3-dB optical coupler, in the forward and backward directions respectively, as defined in Section II A. In order to evaluate the PDL of the DUT, the Jones matrices, $\mathbf{J}$, $\mathbf{B}$ and $\mathbf{F}$, need to be obtained by measuring the Stokes parameters at three linear input polarization states. Then, the Jones matrix of the DUT are

calculated using $\mathbf{A} = \mathbf{B}^{-1}\mathbf{J}\mathbf{F}^{-1}$, where -1 denotes the inverse of a matrix. We can then compute the eigenvalues of $\mathbf{A}^{*t}\mathbf{A}$ and determine PDL_{DUT} according to Equation (4-4):

$$PDL_{DUT} = 10\log\left(\frac{\lambda_2(\mathbf{A}^{*t}\mathbf{A})}{\lambda_1(\mathbf{A}^{*t}\mathbf{A})}\right) = 10\log\left(\frac{\lambda_2(\mathbf{F}^{-1^{*t}}\mathbf{J}^{*t}\mathbf{B}^{-1^{*t}}\mathbf{B}^{-1}\mathbf{J}\mathbf{F}^{-1})}{\lambda_1(\mathbf{F}^{-1^{*t}}\mathbf{J}^{*t}\mathbf{B}^{-1^{*t}}\mathbf{B}^{-1}\mathbf{J}\mathbf{F}^{-1})}\right). \quad (4\text{-}16)$$

The measurement error and the contribution of other components can be evaluated by making a large number of measurements of **J**, **B** and **F** at each wavelength, and calculating the corresponding $PDL_{meas.}$ and PDL_{DUT}. Then the mean variation of the measurement can be obtained by comparison of $PDL_{meas.}$ and PDL_{DUT}. This will be the scope of a future work.

Chapter 5

PMD Measurement Techniques

In this chapter, the wavelength dependency of PMD in fiber gratings and the mean PMD in optical fiber and devices, such as circulators are characterized. Five measurement techniques are introduced and two of them, the measurement setups for the Jones matrix eigenanalysis method and the interferometric method, are implemented, and are discussed, compared and analyzed. Typical measurement results and an uncertainty analysis are presented.

5.1 Definitions of PMD

Definition 1:

The dual-mode nature of singlemode fiber and fiber-optic components gives rise to first order PMD. According to the first definition, PMD is the time of flight or the mean square deviation of the time of flight of the two polarization modes.

$$PMD_1 = \Delta\tau \equiv 2(< t^2 > - < t >^2)^{1/2} = 2\left(\frac{\int I(t)t^2dt}{\int I(t)dt} - \left(\frac{\int I(t)tdt}{\int I(t)dt}\right)^2\right)^{1/2}, \qquad (5\text{-}1)$$

where I (t) denotes the time-dependent intensity at the output of the fiber when a short pulse is launched into the fiber. For polarization-maintaining fibers (PMFs) and many fiber-optic components, I (t) has two peaks and $\Delta\tau$ is the delay between these peaks. In the case of strong polarization mode coupling, I (t) has a quasi-Gaussian shape, $\Delta\tau$ is its full-width-at-half-maximum (FWHM), as shown in Figure 5-1, (refer to Section 5.2.1.1 for details) and can be

expressed in terms of fiber length L, mean coupling length l_c, and the average modal birefringence B:

$$(\Delta\tau)^2 = \frac{B^2 l_c^2}{2}(2L/l_c - 1 + e^{-2L/l_c}). \tag{5-2}$$

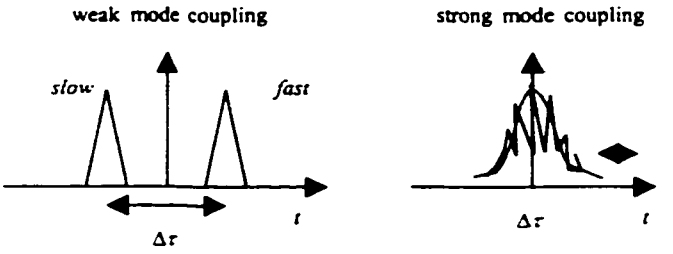

Figure 5-1. Illustration of the PMD in the case of weak and strong mode coupling.

Definition 2:

For fibers used in communication links, the coherence time of the laser source is usually larger than the polarization mode delay defined in definition 1. The output polarization modes will thus interfere. It can be shown that the interference pattern produces two output pulses, both are orthogonally polarized and their polarization states are called the PSPs [62, 70] (refer to Section 3.4 for details on PSP). PMD is then defined as the DGD between these PSPs or the mean DGD over a large wavelength range of interest.

The DGD is wavelength dependent. When the input wavelength/frequency changes, the output polarization rotates about the PSP axis. According to the second definition of PMD, the rate of the rotation is a measure of the DGD, given by:

$$PMD_{II} = << \tau(\omega) >>_{\omega} \equiv \frac{\int_{\omega_1}^{\omega_2} \tau(\omega) d\omega}{\omega_2 - \omega_1}, \text{ or} \tag{5-3a}$$

$$PMD_{II} = \Delta\tau(\omega) \equiv \frac{\Delta\theta}{\Delta\omega} \tag{5-3b}$$

where $\Delta\theta$ is the rotation about the PSP axis in radians, and $\Delta\omega = \omega_2 - \omega_1$ is the optical frequency change.

The relation between the two definitions has been investigated [71,72]. The DGDs between the PSPs, $\tau(\omega)$, are related to the first definition as follows:

$$PMD_I = \Delta\tau = \left(\frac{\int \tau(\omega)_2 d\omega}{\omega_2 - \omega_1} \right)^{1/2} = \sqrt{<< \tau(\omega)^2 >>_\omega} \,. \tag{5-4}$$

For fibers with no/weak mode coupling or with a length less than the coherence length, ($L << l_c$), the DGD, $\Delta\tau$ increases linearly with the fiber length. The PMD coefficient is then expressed as the DGD per unit length

$$PMD_{L<<l_c} = \frac{\Delta\tau}{L} = \frac{<< \tau(\omega) >>_\omega}{L} \text{ (ps m}^{-1}\text{)}. \tag{5-5}$$

For long-length fibers ($L>>l_c$) with strong mode coupling, the statistical distribution of the delay has a Maxwellian distribution [73,74]. The delay $\Delta\tau$ increases with the square root of fiber length, and the PMD coefficient is expressed as the DGD per unit square-root length:

$$PMD_{L>>>l_c} = \frac{\Delta\tau}{\sqrt{L}} = 1.085\frac{<<\tau(\omega)>>_\omega}{\sqrt{L}} \quad (\text{ps km}^{-1/2}). \tag{5-6}$$

Fiber length in the transition region $L \sim l_c$ may require analysis methods beyond the scope of those prescribed here.

The DGD $\Delta\tau$ can be averaged over wavelength, time, or temperature, yielding $<\Delta\tau>_\lambda$, $<\Delta\tau>_t$, or $<\Delta\tau>_T$, respectively. For most purposes, it is not necessary to distinguish between these various options for obtaining $\Delta\tau$. In a system with several individual sources of PMD, the total PMD is a statistical phenomenon that can be estimated as the root-sum-square of the individual PMD elements.

Corresponding to the two PMD definitions, there are two categories of PMD measurement techniques: time-domain measurements and frequency (spectral) domain measurements. The first standard PMD definition, i.e., the time of flight or the mean square deviation of time of flight derived from the time domain principle, is used with the interferometric method [75-78], and optical pulse method [79]. The second definition, i.e., the DGD between the PSPs, or the mean DGD derived from the frequency domain, is used with the extrema-counting wavelength scanning method (also called the fixed analyzer) [80-82], the Jones matrix eigenanalysis method [70,83,84], the Poincare sphere method [85,86], the SOP method [80], the transfer function matrix method [87], and the modulation phase-shift method [88,89].

5.2 Theoretical Background and Experimental Setups

5.2.1 Time-Domain PMD Measurements

5.2.1.1 Interferometric Method

The interferometric method is based on the measurement of the electric-field autocorrelation of two signals derived from the same wideband source. It directly measures the time delay using a Michelson interferometer. The interferometer splits the incoming light into two arms and recombines them at the output. The recombined output intensity is measured when one of the arms is scanned with the other fixed. The scanning arm produces a differential spatial length between the two arms, resulting in a time delay.

For a Michelson interferometer without DUT, shown in Figure 5-2, the interference occurs only when the difference in the lengths of the two arms is less than the coherence length of the source. An autocorrelation peak appears when the lengths of the two arms are equal. The amplitude of the photocurrent envelope is displayed as a function of the time delay introduced by the moving mirror. The width of the response is inversely proportional to the source spectral width. Therefore a broadband source is needed to shorten the coherence length and sharpen autocorrelation peak.

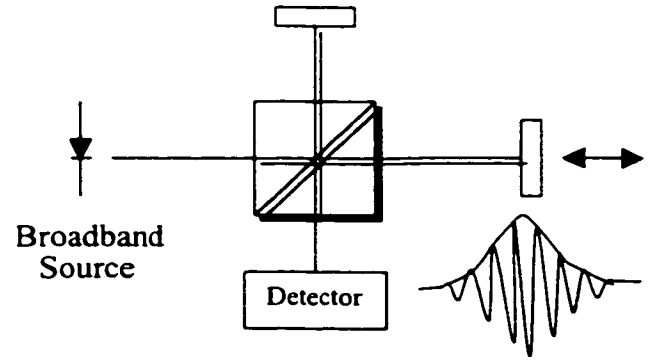

Figure 5-2. Michelson Interferometer.

When a DUT in a weak mode-coupling regime is connected, as shown in Figure 5-3, the input polarized light is split into two polarization modes propagating along the PSP axes. At the output of the DUT these states recombine with a differential delay between them caused by the PMD of the DUT. This signal is then split into two arms, and both are reflected by the mirrors and recombined. When one mirror is scanned, the output response of the interferometer will have three peaks, a central peak corresponding the autocorrelation peak, two side peaks with the distance between them corresponding to the time delay due to the PMD of the DUT. When a broadband source, such as light-emitting diode (LED) is used, the PMD of the DUT, $\Delta\tau$, is simply determined by the spatial length $2\,\Delta L$ between the two side peaks:

$$\Delta\tau = \frac{2\Delta L}{c}. \tag{5-7}$$

By inserting a quarter-wave plate in one arm, as shown in Figure 5-3, the incoming and outgoing light signal from the quarter-wave plate will have 180 degrees phase difference. In the interferometer, the two signals that are 180 degree out of phase interfere with each other and the central peak is cancelled. This increases the resolution of the interferometer and lowers the minimum PMD one can measure.

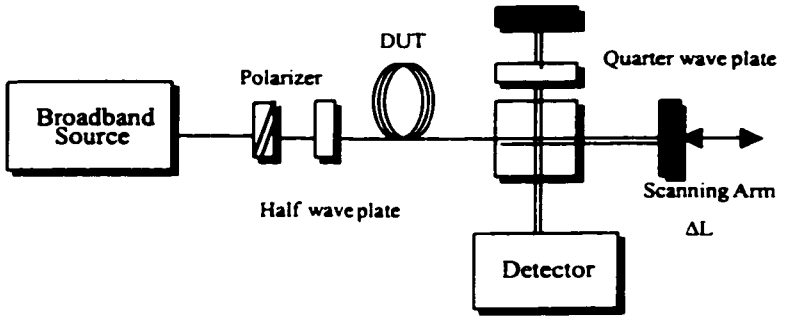

Figure 5-3. Experimental setup for PMD measurement: Interferometric method.

For fibers in the strong polarization mode-coupling regime, fibers with PMD much greater than the coherence time of the source, the envelope of the interferometric response has a nearly Gaussian shape. One can fit a Gaussian curve onto the interferometric response pulse, given by

$$f(x) = \sqrt{\frac{\ln 2}{\pi}} \frac{2}{a} \exp\left\{ - \frac{4(x-b)^2 \ln 2}{a^2} \right\}, \tag{5-8}$$

where b is the center of the fit and the mean DGD is then determined by parameter a, the full-width-at-half-maximum (FWHM) of the fit.

The interferometric method directly provides the measurement of the polarization mode delay. It is not very sensitive to movement and variations during the measurement and has a large dynamic range (see Section 5.4 in this chapter for details). However, it does not provide information about the PSPs.

5.2.1.2 **Optical Pulse Method**

Another time-domain PMD measurement method is the optical pulse method. The experimental setup for the optical pulse method is shown in Figure 5-4. An ultra-short-pulse source and high-speed detector are required. The measurement accuracy depends on the optical pulse width. Since the principal states are measured sequentially, the instrumentation must be extremely stable.

The incident short pulse with respect to the PSP axes of the DUT is launched into the DUT. The output optical pulse is split into two pulses (fast and slow polarization modes). The difference in arrival time of the two pulses emerging with the corresponding output PSPs is measured, which is equivalent to the average PMD value.

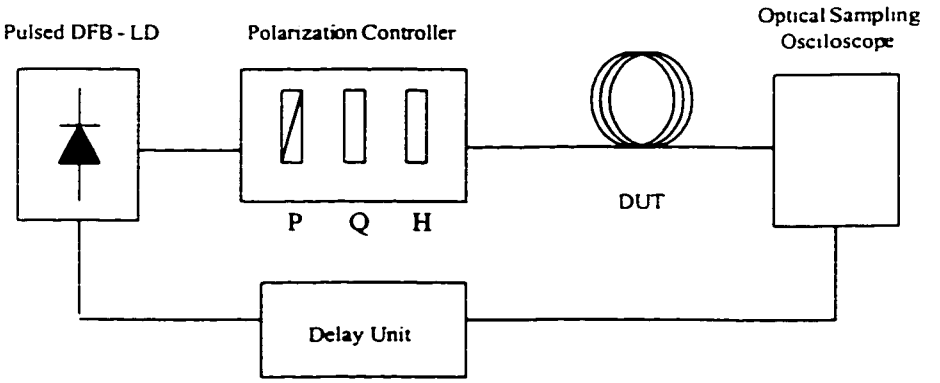

Figure 5-4. Experimental setup for PMD measurement: the optical pulse method.

5.2.2 **Frequency-Domain PMD Measurements**

Most frequency domain methods, such as the Jones matrix eigenanalysis, the wavelength-scanning, the Poincare arc, and SOP methods derive information from the change in output

polarization state of the DUT as wavelength is changed, and the DGD is calculated from Eqn. (5-3b).

5.2.2.1 **Jones Matrix Eigen-Analysis Method**

The Jones matrix eigenanalysis method directly obtains the DGD, $\Delta\tau$, between the PSPs as a function of wavelength. The method is based on the measurement of the transmission/reflection matrix (Jones matrix) of DUT at a set of equally spaced wavelengths over the wavelength range of interest [70,84].

As mentioned in Chapter 2, the transmission/reflection properties of a two-port optical fiber or fiber-optic component can be characterized by its Jones matrix, which relates the input and output Jones vectors. The Jones matrix can be obtained by measuring polarization responses to three input polarization states at a specific wavelength, as shown in Figure 3-2. This process can be repeated over all wavelengths of interest.

According to [62,70], by approximating the derivative of a Jones matrix with respect to frequency and measuring the Jones matrices at two closely spaced optical wavelengths<*Defintion II*, p74>, $\mathbf{T}(\omega)$, $\mathbf{T}(\omega+\Delta\omega)$, the eigen-equation (3-18) becomes:

$$[\mathbf{T}(\omega+\Delta\omega)\mathbf{T}^{-1}(\omega)-(1+i\tau_g\Delta\omega)I]\,\bar{\mathbf{y}}=0 \qquad (5\text{-}9)$$

where τ_g denotes group delay and $\bar{\mathbf{y}}$ is the output Jones vector of the output signal.

The DGD between the PSPs is then determined by differential time delay caused by the phase difference between eigenvalues, given by:

$$\Delta\tau = \left|\tau_{g,1} = \tau_{g,2}\right| = \left|\frac{Arg(\rho_1 / \rho_2)}{\Delta\omega}\right|, \qquad (5\text{-}10)$$

where $\tau_{g,1}, \tau_{g,2}$ denote the group delays for the PSPs, $\Delta\omega$ is the optical frequency change corresponding to the wavelength step, ρ_1, ρ_2 are the eigenvalues of the product of $\mathbf{T}(\omega + \Delta\omega)\mathbf{T}^{-1}(\omega)$, and Arg denotes the argument function, i.e. $Arg(\alpha\varepsilon^{j\theta}) = \theta$. Here eigenvectors corresponding to the eigenvalues locate the principal states. For long fiber with strong mode coupling, the mean DGD value can be obtained by averaging over wavelength.

In order to assure the unambiguous determination of the polarization change produced by the wavelength step, i.e., the rotation of the output polarization state about the principal state axis on the Poincare sphere must not exceed π (180 degrees), one requires that $\Delta\theta < \pi$. The wavelength step $\Delta\lambda$ is then bounded by:

$$\Delta\tau\Delta\lambda < \frac{\lambda^2}{2c}, \qquad (5\text{-}11)$$

and at λ=1550 nm: $\Delta\tau\Delta\lambda$ < 4.0 ps nm. The wavelength step is also lower-bounded by the accuracy requirements of measurement, see Section 5.4.2 for details.

The measurement setup used for characterizing optical components in reflection is the same as shown in Figure 4-2. For measurements in transmission, the 3-dB optical coupler is removed. A polarization analyzer, having a polarization adjuster and a real-time (> 1000 samples/s) polarimeter is used to set three linear input polarization states, measure the Stokes parameters for the three states, calculate the Jones matrices at two adjacent wavelengths and

derive the DGD, i.e., the PMD value. Wavelength-dependent measurements are accomplished by using a very stable tunable laser diode having a high resolution.

The Jones matrix eigenanalysis method is very fast, two to three seconds for one measurement of the Jones matrix at one wavelength, and five to six second for one DGD result. However, the wavelength step for the measurements must be chosen very carefully. For details, refer to section 5.5 of this chapter.

5.2.2.2 **Wavelength-Scanning Method (The Fixed Analyzer Method)**

The wavelength-scanning method, also called the fixed analyzer method, determines PMD from the measurements of output polarization states as a function of wavelength.

It is based on the same idea as the JME method, i.e., over an incremental wavelength change, the rate of rotation around the PSPs as wavelength is changed is a measure of the DGD. It determines the rate of rotation from the number of peaks and valleys in the transmission through a polarizer over a relatively large wavelength range.

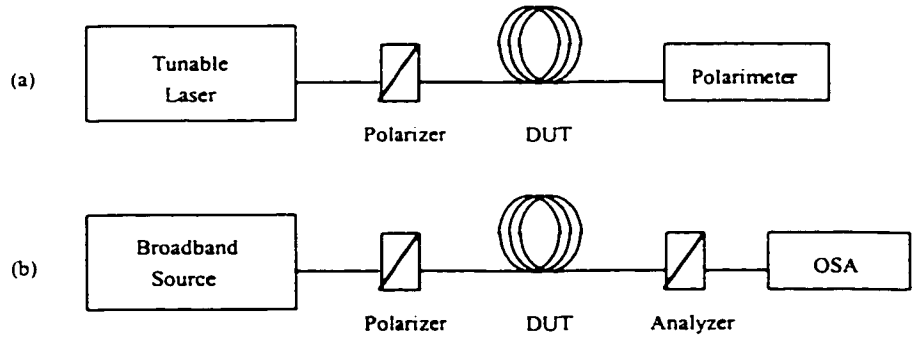

Figure 5-5. Experimental setup for the wavelength-scanning method.

The experimental setup is shown in Figure 5-5 (a). With a polarizer, only that portion of the input signal that is linearly polarized and aligned with the axis of the polarizer can pass through. A polarimeter can be used to measure the normalized Stokes parameters. The mean DGD is then determined by extrema counting from [80]:

$$<\Delta\tau>_{\lambda}=\frac{kN_e\lambda_{start}\lambda_{stop}}{2(\lambda_{stop}-\lambda_{start})c}, \tag{5-12}$$

where N is the number of transmission extrema (peaks and valleys), λ_{start} and λ_{stop} are the endpoints of the wavelength scan, c is the speed of light, and k is the mode-coupling factor that accounts for the effects of the wavelength dependence of the PSP, k = 1 for non-coupled or weakly mode-coupled fiber and components or k = 0.824 for strongly or randomly mode coupled devices.

In an alternative setup, shown in Figure 5-5 (b), a broadband light source is used instead of a tunable laser, and the polarimeter replaced by an optical spectrum analyzer (OSA). Here a reference measurement without the analyzer may be required to account for the wavelength dependence of the optical source output power or the test path insertion loss.

To ensure full resolution of the variations of output polarization with wavelength, the optical source width in either setup should satisfy the condition:

$$\frac{\Delta\lambda}{\lambda}<\frac{1}{8\nu\Delta\tau}, \tag{5-13}$$

where $\Delta\lambda$ is the spectral width of the source or the resolution bandwidth of the receiver, λ is the nominal measurement wavelength, both in meters, ν is the optical frequency in Hz, and $\Delta\tau$ is the DGD of the DUT in seconds. In the region of 1550 nm, Eqn. (5-13) becomes $\Delta\lambda$ [nm] < $1/\Delta\tau$ [ps].

The scanned wavelength range should be large enough to produce a statistically significant number of extrema. For measurements near 1550 nm, the wavelength interval required to generate one cycle (or two peaks) in the output polarization response is given by:

$$\Delta\lambda_{p-p} = \frac{\zeta\,[\text{ps - nm}]}{\Delta\tau\ [\text{ps}]}, \tag{5-14}$$

where ζ = 7.8 for non or weakly mode-coupled devices and ζ = 6.5 for strongly or randomly mode-coupled devices.

The wavelength-scanning method is faster than the Jones matrix eigenanalysis method and easy to implement. It gives only the average DGD, not wavelength-dependence, and it is sensitive to vibrations and launch polarization conditions. No information about the principal states is given and there exists a tradeoff between the spectral width and the wavelength range.

5.2.2.3 **The Modulation Phase-Shift Method**

As a modified version of the phase-shift method used for chromatic dispersion measurements [90,91], the modulation phase-shift method determines the DGD from the difference in modulation phase between the PSPs.

The experimental setup for this method is shown in Figure 5-6. In this setup, a network analyzer is used to generate the RF signal, detect and normalize the phase. A polarization controller is used to convert the fixed input polarization state to all possible polarization states. At each wavelength of interest, while the polarization controller is rotating with a quasi-random pattern, a modulated lightwave with different polarization states is coupled into the DUT, the emerging light is detected by an optical detector, and sent to the network analyzer. A computer is used to collect the phase data, search for the maximum and minimum phase, and calculate the DGD at each wavelength via:

$$\Delta\tau(\lambda_i) = \frac{\phi_{\max}(\lambda_i) - \phi_{\min}(\lambda_i)}{360 \times f_m} \times 10^{12} \qquad \text{[ps]}, \tag{5-15}$$

where $\{\lambda_i\}$, i =1,2, ..., N, each one refers to the central wavelength of the wavelength step within the range of interest, f_m is the RF modulation frequency in Hz , $\phi_{\max}$ and $\phi_{\min}$ are the maximum and minimum phase shifts.

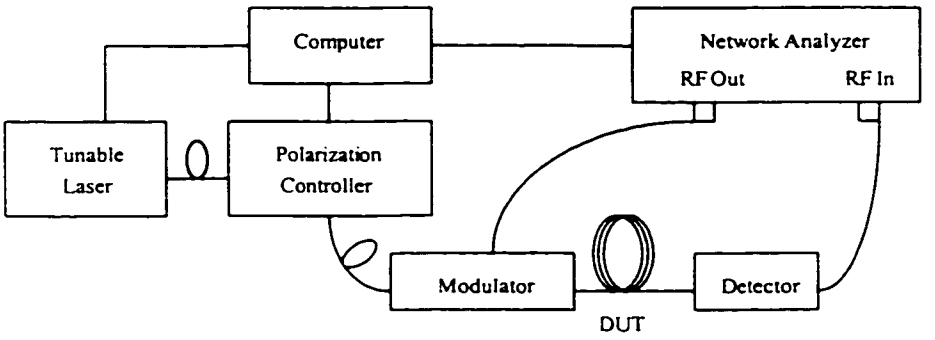

Figure 5-6. Modified modulation phase-shift method for PMD measurement.

The modulation phase-shift method is simple and can also be used for PDL measurements [88, 89]. However, it requires both temperature stability and physical stability. A calibration procedure may be required to account for the phase noise induced by the instrumentation and connecting fibers.

5.3 Measurement Results and Discussion

5.3.1 Choosing PMD Measurement methods

All the techniques described in the previous section can be used to measure the mean DGD in either the time domain or the frequency domain. The Jones matrix eigenanalysis method can even be used to measure the wavelength dependency of the DGD. Which method is to be chosen depends on the PMD value of the DUT, the availability of the instrumentation, as well as the characteristics of each method, outlined below.

The optical-pulse method determines the PMD from the direct measurement of the change in pulse arrival time, and gives a clear picture of optical pulse broadening. However, it is crucially dependent on the stability of the instrumentation and the width of the short pulse, and offers no wavelength dependence information of the PMD. This method is suitable for measurements in long polarization-maintaining fibers (PMFs) and high birefringent optical components with large PMD values, not suitable for optical components with small PMD values, such as dispersion compensation gratings, WDM grating filters, etc.

The interferometric method determines the PMD from the electric field autocorrelation function using a broadband source and a Michelson interferometer. The mean DGD can be obtained simply by scanning one of the reflection mirrors. This method has large dynamic range, and is insensitive to perturbation of the measurement setup. It is suitable for mean DGD

measurements in PMFs, birefringent optical components, short-fibers (SMF, DSF, etc.), but not in narrowband optical components such as FBGs.

The Jones matrix method determines the DGD from the measured Jones matrices at two adjacent wavelengths. It offers information about the PSPs, the wavelength dependency of the DGD, as well as the mean DGD over the wavelength range of interest. With an appropriate wavelength step (see Section 5.4.1 for details), this method is suitable for wavelength dependency as well as mean DGD measurements in optical fibers, wavelength-selective narrowband devices, such as fiber gratings, as well as other kinds of fiber-optic devices.

The wavelength-scanning (fixed analyzer) method determines the DGD from the random evolution of the output polarization states as wavelength is scanned. It is suitable for mean DGD measurements in optical fibers, fiber-optic components, and optical amplifier systems, etc. However, it offers no information about the PSPs, and the measurement accuracy is affected by the scanned wavelength range.

The modulation phase-shift method determines PMD at a wavelength from measurements of the change in modulation phase between the PSPs. The wavelength dependency measurement can be achieved by using a tunable laser source. It is suitable for measurements in optical fibers and fiber-optic devices. However, the minimum PMD that can be measured depends on the background noise of the network analyzer, making it unattractive for the measurement of devices with ultra-low PMD values.

Based on these facts, in this thesis, two PMD measurement techniques have been chosen: (a) the Jones matrix eigenanalysis method to measure the wavelength-dependency of PMD in fiber gratings, as well as the mean DGD in fibers and optical devices, such as circulators; and

(b) the interferometric method to measure the mean PMD in broadband (non-wavelength-selective) devices.

5.3.2 **Measurement Results**

As mentioned above, we have implemented the Jones matrix eigenanalysis method to measure the wavelength-dependent PMD and mean PMD, and the interferometric method to measure the mean PMD of passive optical components, used in reflection or transmission as shown in Figures 4-2 and 5-3. A stable wavelength tunable laser diode TUNICS-PRI from Photonetics and a HP8509B polarization analyzer were used in the experimental setup for the Jones matrix eigenanalysis method. The polarization analyzer consists of a polarization adjuster, three linear polarizers, and a polarimeter. Before the measurements, the polarization adjuster has to be set to provide roughly circularly polarized light, so that the polarizers never become cross polarized with respect to the input light.

A LED/Opreal Broadband light source, a Newport PM500 Precision Motion Controller, and a HP8153 Lightwave multimeter with an HP81533B Optical Head were used for the experimental setup for the interferometric method. Optical connectors were used to connect the DUT to the set-up.

The fiber cables/pigtails and fiber-optic components in the setups must not be moved during the measurements to avoid changes in the polarization state passing through these components, especially for the Jones matrix eigenanalysis method. For the interferometric method, the movable mirror on a stage is scanned by the precision motion controller with a very small step of 0.1 micron. For the Jones matrix eigenanalysis method, the wavelength was scanned over the wavelength range of interest using an appropriate step, which depends on the

transmission or reflection bandwidth of the device. Narrowband, single-channel fiber Bragg gratings for dispersion compensation and WDM grating filters for wavelength add/drop multiplexing have been characterized using a wavelength step of 0.01 nm, while broadband devices such as long period gratings for gain flattening of EDFAs have been characterized using a 0.2 nm step size.

The wavelength-dependent PMD of a chirped fiber Bragg grating, used in reflection as a dispersion compensator, and a grating filter, used in reflection for WDM add/drop multiplexing, have been measured using the setup for the Jones matrix eigenanalysis method, as shown in Figure 4-2. The results are shown in Figures 5-7 and 5-8 respectively. The measured reflection responses are also shown for reference. It can be seen that the measured PMD is very high outside the 3-dB reflection bandwidth due to the lower power level and the large ripples in the reflection response. The typical PMD values within the 3-dB bandwidth of the dispersion compensation gratings are high, varying from 0.5 to 10 ps. The repeatability of the measurement results can be observed in Figure 5-7. The typical PMD values of the WDM grating filter are much lower within its 3-dB bandwidth, varying from 0.04 to 0.8 ps.

The 3-dB bandwidths of the dispersion compensation grating and the WDM grating are small, about 0.6 nm and 0.8 nm respectively, and in this case the wavelength dependence of the setup is negligible. The input circular polarization was adjusted at the central wavelength.

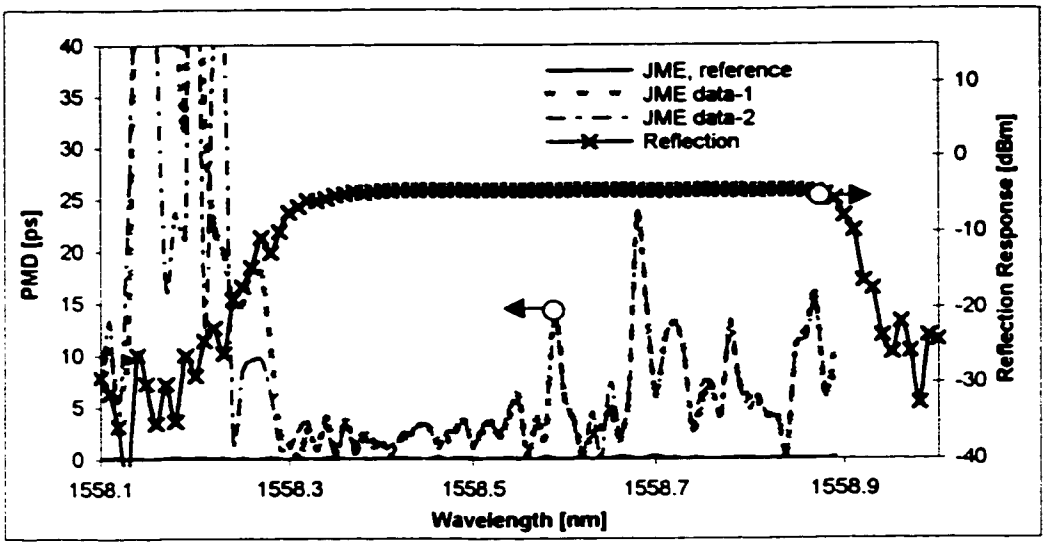

Figure 5-7. Measurement results for a dispersion compensation grating. The wavelength-dependant PMD is measured using the Jones matrix eigenanalysis (JME) method. The system PMD (JME reference) and the reflection response are shown for reference.

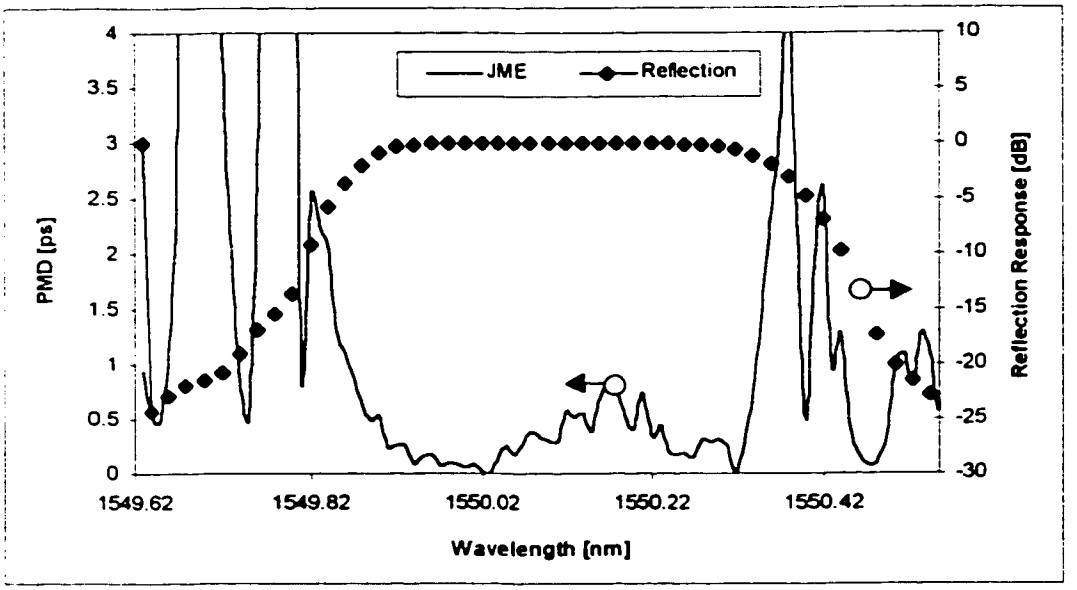

Figure 5-8. Measurement results for a WDM grating filter. The wavelength-dependent PMD is measured using the Jones matrix eigenanalysis (JME) method. The reflection response is shown for reference.

The wavelength-dependent PMD of a long period grating used in transmission for EDFA gain flattening has been obtained using the setup shown in Figures 4-2. In this case the 3dB fiber optic coupler was removed and the device connected directly to the optical input and output ports of the polarization analyzer. Figure 5-9 shows the measured wavelength-dependent PMD and transmission response for the long period grating. As observed from Figure 5-9, this grating has a smooth spectral response. The measurements were performed using a wavelength step of 0.2 nm. For the measured long period gratings with a 3-dB bandwidth of about 30 nm, the input circular polarization state was readjusted every 5 nm to account for the wavelength dependency of polarization in the system.

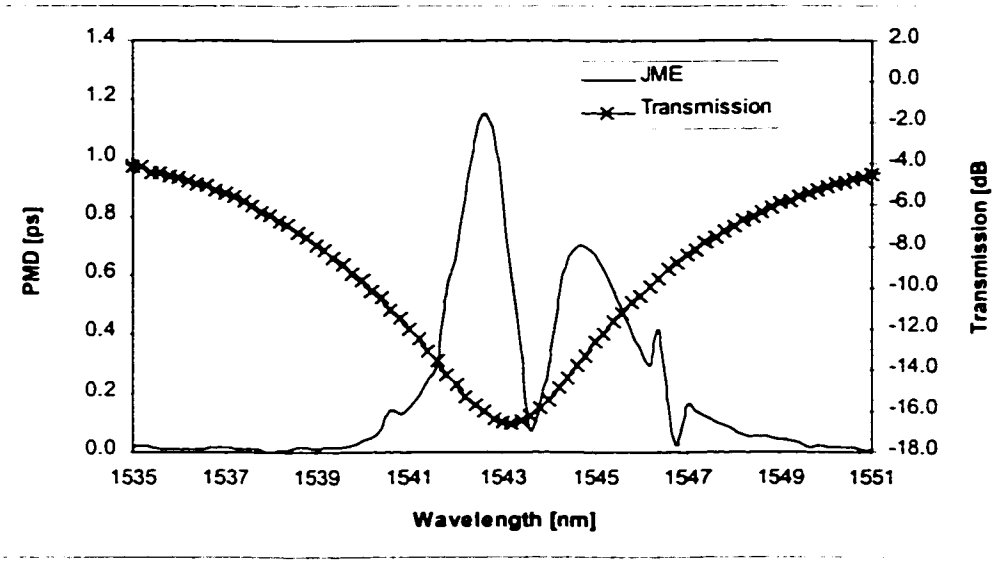

Figure 5-9. Measurement results for a long period grating. The wavelength-dependant PMD is measured using the Jones matrix eigenanalysis (JME) method. The transmission response is shown for reference.

The PMD of a circulator used in transmission has been measured using the setup shown in Figures 4-2 and 5-3. In this case the 3dB fiber optic coupler was removed. The measurement results are shown in Figure 5-10, where (a) shows the wavelength dependence of the PMD in the circulator obtained from the Jones matrix eigenanalysis method, and (b) shows the interference pattern obtained by using the interferometric method. In Figure 5-10 (b), it can be observed that the two peaks obtained are clearly separated. The mean DGD of the circulator with no mode coupling, can be determined through Eqn. (5-7), giving a mean DGD about 0.072 ps. From Figure 5-10 (a), the mean PMD averaged over wavelength is 0.075 ps. A good agreement has been obtained between these two methods with a discrepancy of 0.003 ps.

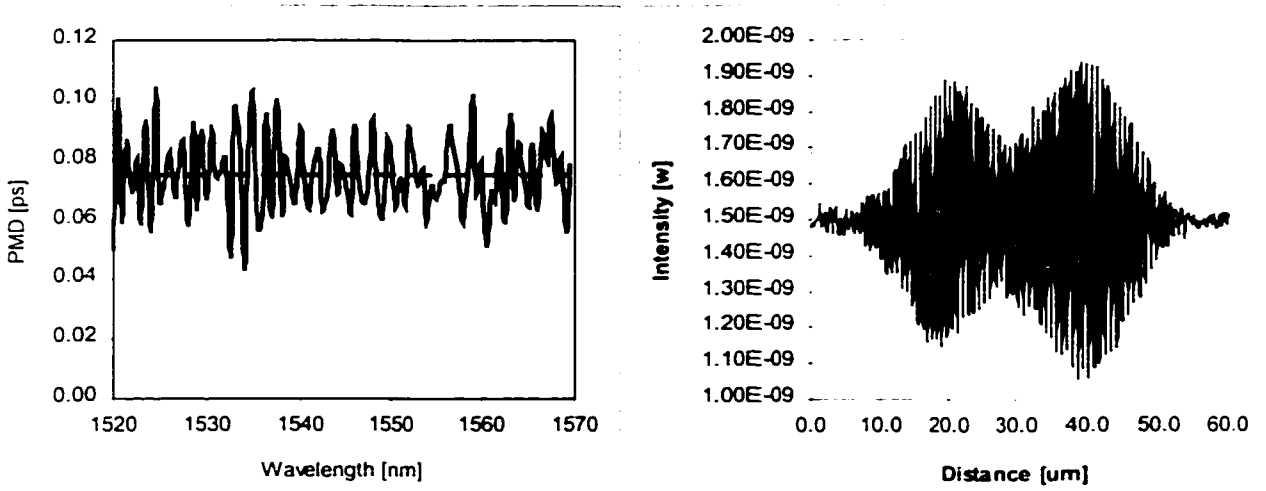

Figure 5-10. Measurement results for a circulator, (a) using the Jones matrix eigenanalysis (JME) method, and (b) using the interferometric method.

The PMD of a fiber with a length of about 11.8 km has been measured using the setup shown in Figures 4-2 and 5-3. In this case the 3dB fiber optic coupler was removed. The

measurement results are shown in Figure 5-11, where (a) shows the wavelength dependence of PMD in the fiber obtained from the Jones matrix eigenanalysis method, and (b) shows the interference pattern obtained by using the interferometric method. In Figure 5-11 (b), it can be observed that the two main peaks separated are accompanied by sidelobes resulting from some degree of mode coupling. The mode coupling is not strong enough to justify using a Gaussian fit to the interference pattern. The mean DGD can also be determined through Eqn. (5-7), where $2\Delta L$ corresponding the distance between the two main peaks, giving a mean DGD about 0.0217 ps. From Figure 5-11 (a), the mean PMD averaged over wavelength is 0.0229 ps. A good agreement has been obtained between these two methods with a discrepancy of 0.012 ps.

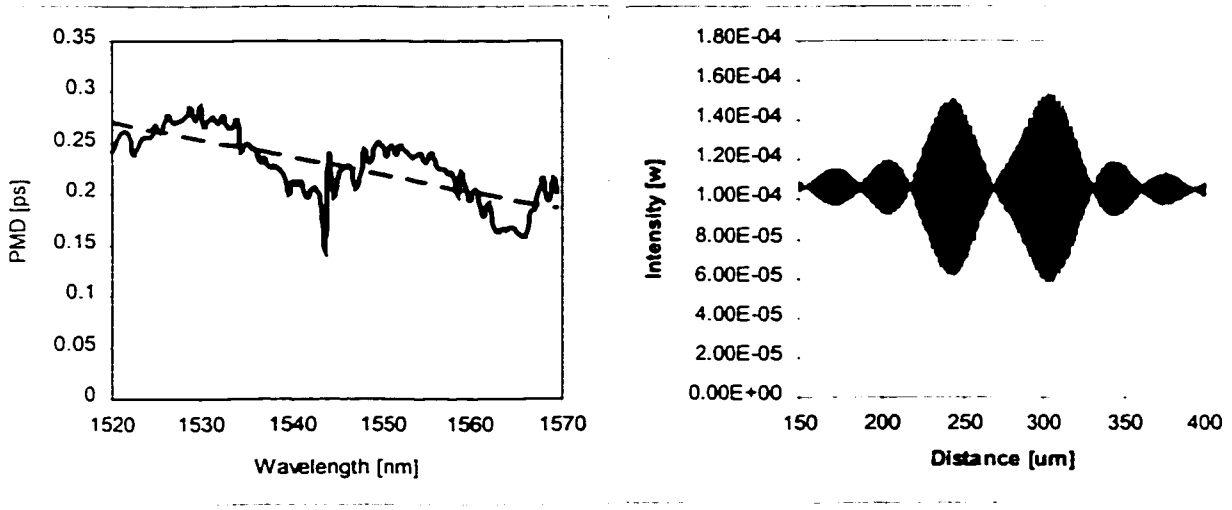

Figure 5-11. Measurement results for a 11.8 km spool of fiber, (a) using the Jones matrix eigenanalysis (JME) method, and (b) using the interferometric method.

The PMD of a fiber with a length of about 24 km has been obtained using the setup shown in Figures 4-2 and 5-3. In this case the 3dB fiber optic coupler was removed. The measurement results are shown in Figure 5-12, where (a) shows the wavelength dependence of PMD in the

fiber obtained from the Jones matrix eigenanalysis method, and (b) shows the interference pattern obtained by using the interferometric method. In Figure 5-12 (b), strong mode coupling effects can be observed. One then can use Eqn (5-8) to fit a Gaussian curve into the intensity response obtained. The FWHM gives a mean DGD of about 0.393 ps. From Figure 5-12 (a), the mean PMD averaged over wavelength is 0.41 ps. A good agreement has been obtained between these two methods with a discrepancy of 0.017 ps.

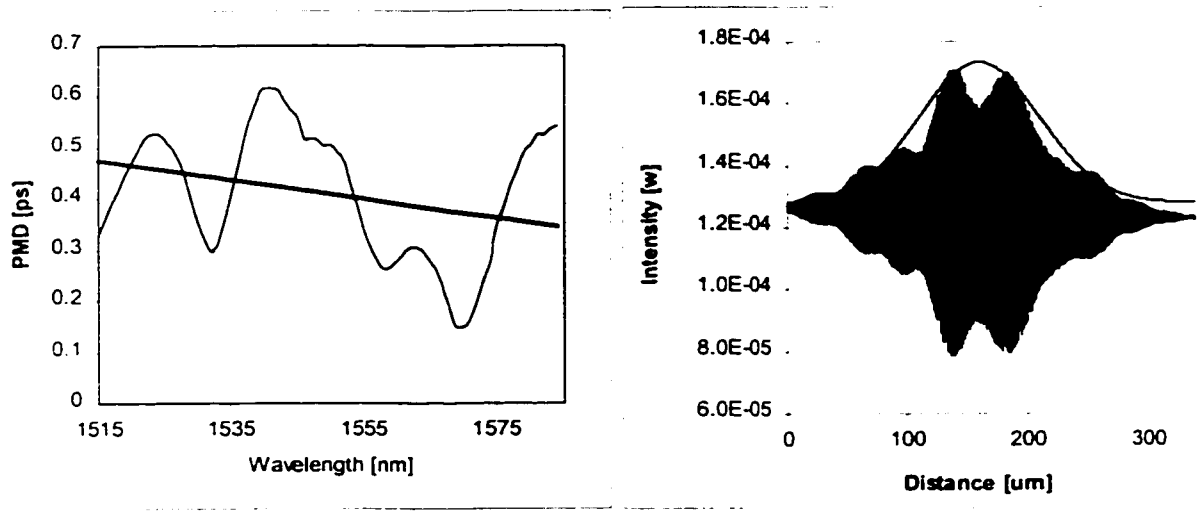

Figure 5-12. Measurement results for a 24 km spool of fiber, (a) using the Jones matrix eigenanalysis (JME) method, and (b) using the interferometric method.

5.4 Accuracy and Measurement Error

The major sources of PMD errors have to be taken into account. These sources include the laser tuning linearity and repeatability and the angle step of the polarizers in the polarization analyzer for the Jones matrix eigenanalysis method, the scanning step of the precision motion controller and the spectrum width of the broadband light source for the Interferometric method.

Thermal instabilities may also affect the accuracy of the measured PMD and increase the uncertainty in the measurement results. At least one hour of warm-up time is needed for most instruments to achieve thermal stabilization. Fiber cables and fiber-optic components in the measurement setups must not be moved during a measurement to ensure that the polarization transfer function of the components remains unchanged, especially for the Jones matrix eigenanalysis method. Usually a few minutes waiting time is sufficient for the fiber components to stabilize after they are disturbed. Connector pairs cause reflections at the connector interface and increase the uncertainty in the measured PMD. Proper care of the connectors and fusion spliced connections can reduce the PMD uncertainty. To measure a device used in reflection, another optical component, a 3-dB coupler or a circulator must be added to the measurement setup, which increases the uncertainty of the measurements.

5.4.1 **The Jones Matrix Eigenanalysis Method**

The major sources of error in the Jones matrix eigenanalysis method originate from the degree of polarization (DOP) of the light source, the laser tuning linearity and repeatability, and the angle step of the polarization analyzer.

The spectral distribution of the tunable laser source should be narrow enough to insure that light emerging from the DUT remains polarized under all measurement conditions. A DOP of 90 % or greater is preferred.

The wavelength step also affects the measurement accuracy. As mentioned in Section 5.2.1, the wavelength step $\Delta\lambda$ is bounded by the unambiguous determination of the output polarization state over the wavelength step, giving by Eqn. (5-10). $\Delta\lambda$ also must be larger than a

certain value in order to obtain a satisfactory measurement accuracy. From Eqn. (5-3b), the relative measurement error of the DGD can be expressed as:

$$\frac{\delta\Delta\tau}{\Delta\tau} = \frac{\delta\Delta\theta}{\Delta\theta} \pm 2\frac{\delta\lambda}{\lambda} \pm \frac{\delta\Delta\lambda}{\Delta\lambda}, \tag{5-16}$$

where $\delta / \delta\Delta$ denote the measurement error, $\delta\Delta\theta$ is the phase angle error, $\delta\Delta\lambda$ is the wavelength step error.

The second term in Eqn. (5-15) is negligible since the relative error in wavelength is much smaller than the phase angle error and the wavelength step error. The phase error is determined by the position repeatability of the polarizer (in the polarization analyzer), which is ± 1 degree.

For example, $\delta\Delta\lambda = \pm 0.005\,\text{nm}$, $\delta\Delta\theta = \pm 1^{\circ}$, $\Delta\lambda$ was chosen to be 0.2 nm for long period grating measurements, which gave an accuracy of at least 3%.

5.4.2 **The Interferometric Method**

The major sources of error for the interferometric method come from the coherence time of the light source, the launched state of polarization, the step resolution of the moving arm.

The coherence time, τ_c, of an optical source is a measure of the spectral purity of the laser frequency over time. In two-path interferometers, the degree to which an optical wave interferes with a time-delayed portion of itself depends on the coherence time of the wave with respect to the optical delay. The related concept coherence length l_c, is simply the coherence time multiplied by the velocity of light: $v_g = c / n_g$, where n_g, the group velocity index, is 1 in free space. The coherence length l_c is given by:

$$l_c = \frac{\lambda^2}{\Delta\lambda_c}, \tag{5-17}$$

where $\Delta\lambda_c$ is the spectral linewidth the source.

The coherence length determines the width of the intensity peaks in the interference pattern. Combined with the minimum step resolution of the moving arm, it determines the minimum measurable PMD value, while the maximum measurable PMD value is determined by the scanning range of the adjustable arm.

The repeatability of the autocorrelation function depends on both input and output states of polarization of the DUT. For various launch conditions, the corresponding correlation functions yield to a standard deviation of about 15 % [79].

The step resolution of the moving arm also gives a rise to the instrument uncertainty. The instrument uncertainty is given by

$$\delta\Delta\tau = \frac{2}{c}\delta\Delta L, \tag{5-18}$$

where δ denotes the measurement error. For example, 3 micron distance scanned for the adjustable arm used may result in 0.01 ps PMD error.

Chapter 6

Conclusions

6.1 Summary

The goals of this thesis were to investigate, implement, assess and compare different PMD and PDL measurement techniques and to measure these quantities in a number of optical devices including fiber gratings. These tasks were accomplished and are outlined below.

First, an overview of fiber gratings, including theoretical background, fabrication techniques and their applications in optical fiber telecommunication systems was presented in order to help the readers fully understand fiber gratings' properties, behavior, and the importance of their characterization.

Secondly, three calculational tools, i.e., the Jones calculus, the Mueller calculus, and the Poincare sphere were introduced to quantitatively describe the interaction of light with optical devices. They can be used to calculate the polarization properties of the devices, such as PMD and PDL. A PSP model was also presented, which was used to describe the polarization dispersion for long fibers.

Then, we have characterized, for the first time, the wavelength dependency of PDL in three types of fiber gratings commonly used in optical fiber communication systems: chirped fiber Bragg gratings for dispersion compensation, WDM grating filters for add/drop multiplexing, and long period gratings for gain compensation. Three measurement set-ups for the Jones matrix method, the Mueller matrix method, and the polarization scanning method, have been discussed, implemented, compared and analyzed. Different calibration procedures were performed to account for the systems' PDL and the strong wavelength dependency of the

setups. Typical measurement results in these fiber gratings and an uncertainty analysis have been presented.

Five PMD measurement techniques, the interferometric, the optical pulse, the Jones matrix eigenanalysis, the wavelength-scanning, and the modulation phase-shift methods were reviewed. Two experimental techniques, i.e., the Jones matrix eigen-analysis and the interferometric method used to characterize the wavelength-dependent PMD in fiber three types of fiber gratings, and the mean PMD in singlemode spooled fibers and optical circulators, were implemented and compared. Typical experimental results were presented, compared, and discussed. An assessment of accuracy and measurement error was also presented for each of the techniques applied.

6.2 Suggestions for Future Work

1. Evaluating the measurement error and the PDL contributions by making a large number of measurements to obtain the forward and backward Jones matrices of the coupler, as well as the Jones matrix of the DUT combined with the coupler at each wavelength, as mentioned in Section 4.3.1 and 4.4.3.
3. Using electromagnetic numerical modeling techniques to investigate fiber gratings and other optical devices will help to validate theoretical predictions, such as reflectivity and transmission, with the values measured.
4. Development of precise PMD/PDL/chromatic dispersion in-field measurement systems is necessary to upgrade existing fiber systems.
5. Investigation of the possibility of in-field PMD measurement-compensation systems.

6.3 Contributions

- For the first time, the wavelength dependency of PDL in three types of fiber gratings commonly used in optical fiber communication systems have been characterized using three measurement techniques.
- Different calibration procedures have been used and an assessment of measurement uncertainties has been presented for each of the techniques applied.
- Two methods, JME and IF, have been compared and measurement results agree very well.

References

[1] P. E. Green, "Optical Networking Update", IEEE J. Selected Areas in Communications, vol. 14, No. 5, pp.764-779, 1996.

[2] P. Hernday, ch.12, "Dispersion Measurements", Fiber Optic Test and Measurement, Ed. Dennis D. Derickson, Prentice Hall, 1998.

[3] Darcie, T.E. and C.D. Poole, "Polarization-induced performance variables", Communications Engineering and Design, 1992.

[4] Bassoon, S., J. Nagel, and C. Poole, "Measurements of temporal variations in fiber transfer characteristics to 20 GHz due to polarization-mode dispersion, Proc. 16th European Conf. Opt. Comm., Amsterdam: pp.1003-1006, 1990.

[5] Poole, C.D., R.W. Tkach, A.R. Chraplyvy, and D.A. Fishman, "Fading in lightwave systems due to polarization-mode dispersion", IEEE Photonics Technology Letters, 3: pp. 68-70, 1991.

[6] N. Gisin, B. Huttner, "Combined effects of polarization mode dispersion and polarization dependent losses in optical fibers", Optics Communications 142: pp. 119-125, Oct., 1997.

[7] L. G. Kazovshy, A. F. Elrefaie, R. Welter, P. Crepso, J. Gimlett, and R.W. smith, "Impact of laser intensity noise on ASK two-port optical homodyne receivers", Electron. Lett, vol. 23, pp. 871-873, 1987.

[8] T. Georges and F. Fabre, "Influence of solition interaction on amplifier noise-induced jitter: a first-order analytical solution", Opt. Lett. Vol. 16, No. 21, page 1656, 1991.

[9] P. V. Mamyshew and L. F. Mollenauer, "Pseudo-phase-matched four-wave mixing in soliton wavelength-division multiplexing transmission", Opt. Lett., 21, page 396, 1996.

[10] T. Georges and B. Charbonnier, "Reduction of the dispersive wave in periodically amplified links with initially chirped solitons", IEEE Photonics Technology Letters, vol. 9, page 127, 1997.

[11] J. M. Jacob, E. A. Golovchenke, A. N. Pilipetskii, G. M. Garter, and C. R. Menyuk, "Experimental demonstration of soliton transmission over 28 Mm using mostly normal dispersion fiber", IEEE Photonics Technology Letters, vol. 9, pp.130,1997.

[12] K. O. Hill, Y. Fujii, D. C. Johnson, and B. S. Kawasaki, "Photosensitivity in optical waveguides: Application to reflection filter fabrication", Appl. Phys. Lett., vol. 32, no. 10, page 647, 1978.

[13] V. Mizrahi and J. E. Sipe, "Optical properties of photosensitive fiber phase gratings", J. Lightwave Technol., vol. 11, pp. 1513-1517, Oct. 1993.

[14] R. Kashyap, "Photosensitive optical fibers: Devices and applications", Optic. Fiber Technol., vol. 1, pp. 17-34, 1994.

[15] Kenneth O. Hill, "Photosensitivity and its application to optical fiber communications", OFC'95, February 26-March 3, San Diego, California, tutorial Sessions, pp. 146-193, 1995.

[16] G. Meltz, W. W. Morey, and W. H. Glenn, "Formation of Bragg gratings in optical fibers by a transverse holographic method", Opt. Lett., vol. 14, pp. 823-825, 1989.

[17] Anderson, D. Z., Mizrahi, V., Erdogan, T., and white, A. E., "Production of in-fiber grating using a diffractive element", Electron. Lett., 29, (6), pp. 566-568, 1993.

[18] Malo, B., Johnson, D. C., Bilodeau, F., Alert, J., and Hill, K. O., "Single-excimer-pulse writing of fiber gratings by use of a zero-order nulled phase masks: grating spectral response and visualization of index perturbations", Opt. Lett., 18, (15), pp. 1277-1279,

1993.

[19] J. Martin and F. Ouellette, "Novel writing technique of long and highly reflective in-fiber gratings", Electron., Lett., vol. 30, no. 10, pp. 811-812, 1994.

[20] Malo, B., Hill, K. O., Bilodeau, F., Johnson, D. C., and Albert, J., "Micro-Bragg grating in photosensitive fiber using single excimer pulse refractive index modification techniques", Electron. Lett., vol. 29 (18), pp. 1668-1669, 1993.

[21] G. A. Ball, and W. W. Morey, "Continuously tunable singlemode erbium fiber laser", Opt. Lett. vol. 17, pp. 420-422, 1992.

[22] J.A.R. Williams, I. Bennion, K. Sugden, and N. J. Doran, "Fiber dispersion compensation using a chirped in-fiber Bragg grating", Electron. Lett., vol. 30, pp. 985-987, 1994.

[23] C. R. Giles, R. d. Feldman, T. H. Wood, M. Zirngibl, G.Raybon, T. Stulz, A. McCormick, C. H. Joyner, and C. R. Doerr, "Access PON using downstream 1550-nm WDM routing and upstrem 1330-nm SCMA combining through a fiber-grating router", IEEE Photon. Technol. Lett., vol. 8, pp. 1549-1551, Nov. 1996.

[24] C. R. Giles and V. Mizrahi, "Low-loss add/drop multiplexers for WDM lightwave networks", in Proc. IOOC'95, Hong Kong, 1995, paper ThC2-1.

[25] K. O. Hill, B. Malo, K. A. Vineberg, F. Bilodeau, D. C. Johnson, and I. Skinner, "Efficient mode conversion in telecommunication fiber using externally written gratings", Electron. Lett., vol.26, pp. 1270-1272, 1990.

[26] B. F. Ventrudo, G. A. Rodgers, G. S. Lick, D. Hargreaves, and T. N. Demayo, "Wavelength and intensity stabilization of 980 nm diode lasers coupled to fiber Bragg gratings", Electron. Lett., vol. 30, pp. 2147-2149, 1994.

[27] P. A. Morton, V. Mizrahi, S. G. Kosinski, L. F. Mollenauer, T. Tanbun-Ek, R. A. Logan,

D. L. Coblentz, A. M. Sergent, and K. W. Wecht, "Hybrid soliton pulse source with fiber external cavity and Bragg reflector", Electron. Lett., vol. 28, pp. 561-562, 1992.

[28] J. Capmany, D. Pastor, and J. Marti, "EDFA gain equalizer employing linearly chirped apodized fiber gratings", Microwave and Optic. Technol. Lett., 2, pp. 156-160, 1996.

[29] Eric Udd, editor, *Fiber Optic Sensor*, Wiley, New York, 1991.

[30] H. Zmuda, R. A. Soref, P. Payson, S. Johns, and E. N. Toughlian, "Photonic beamformer for phased array antennas using a fiber grating prism", IEEE Photon. Technol. Lett., vol. 9, pp. 241-243, 1997.

[31] C. M. De Sterke, N. G. R. Broderick, B. J. Eggleton, and M. J. Steel, "Nonlinear optics in fiber gratings", Optic. Fiber Technol., vol. 2, pp. 253-268, 1996.

[32] J. Sakai and T. Kimura, "Birefringence and polarization characteristics of single-mode optical fibers under elastic deformations", IEEE J. Quantum Electronics, vol. 17, No.6, page 1041, 1981.

[33] L. P. Kaminow, T. L. Koch, Optical Fiber Telecommunications, Vol. IIIA, Academic Press, 1997.

[34] C. D. Poole and R. E. Wagner, "Phenomenological approach to polarization dispersion in long single-mode fiber", Electron. Letters, vol. 22, No. 19, page 1029, 1986.

[35] T. Erdogan, "Fiber Grating Spectra", J. Lightwave Technol., vol. 15, pp. 1277-1294, 1997.

[36] H. Kogelnik, "Filter response of non-uniform almost-periodic structures", Bell Sys. Tech. J., vol. 55, pp. 109-126, 1976.

[37] L. A. Weller-Brophy and D. G. Hall, "Analysis of waveguide gratings: Application of Rouard's method," J. Opt. Soc. Amer. A, vol. 2, pp. 863-871, 1985.

[38] M. Yamada and K. Sakuda, "Analysis of almost-period distributed feedback slab waveguides via a fundamental matrix approach", Appl. Opt., vol. 26, pp. 3474-3478, 1987.

[39] E. Peral, J. Capmany, and J. Marti, "Iterative solution to the fiber gratings," IEEE, J. Quantum Electron. Vol. 32, pp. 2078-2084, 1996.

[40] A. Yariv, "Coupled-mode theory for guided-wave optics," IEEE J. Quantum Electron., vol. QE-9, pp. 919-933, 1973.

[41] D. Marcuse, *Theory of Dielectric Optical Waveguides*, Academic Press, New York, 1974.

[42] H. Kogelnik, "Theory of optical waveguides," in *Guided-Wave Opto-electronics*, T. Tamir, Ed. New York: Springer-Verlag, 1990.

[43] T. Erdogan, "Cladding-mode resonances in short- and long-period fiber grating filters", J. Opt. Soc. Am. A, vol. 14, pp. 1760-1773, 1997.

[44] W. H. Loh, R. I. Laming, A. d. Ellis, and D. Atkinson, "10 Gb/s transmission over 700 km of standard single-mode fiber with 10-cm chirped fiber grating compensator and duobinary transmitter", IEEE Photon. Technol. Lett., 8, page 1258, 1996.

[45] T. Erdogan, and J. E. Sipe, "Tilted fiber phase gratings", J. Opt. Soc. Am. A., vol. 13, pp. 296-312, 1996.

[46] R. Kashyap, R. Wyatt, and R. J. Campbell, "Wideband gain flattened erbium fiber amplifier using a photosensitive fiber blazed grating", Electron. Lett., vol. 29, pp. 154-156, 1993.

[47] Malo, B., Hill, K. O., Bilodeau, F., Johnson, D. D., and Albert, J., "Point-by-point fabrication of micro-Bragg grating in photosensitive fiber using single excimer pulse refractive index modification techniques", Electron. Lett., vol. 29, pp. 1668-1669, 1993.

[48] P. J. Lemaire et al. "High-temperature stability of phase gratings in GeO_2 -doped optical fibers", OFC'93, San Jose, Calif., Tech. Dig. Paper FA7, 1993.

[49] R. M. Atkins et al., "248 nm induced vacuum UV spectral changes in optical fiber perform cores: Support for a color center model of photosensitivity", Electron. Lett. 29, pp. 385-387, 1993.

[50] H. Patrick, and S. L. Gilbert, "Growth of Bragg gratings produced by continuous-wave ultraviolet light in optical fiber", Opt. Lett., vol. 18, pp. 1484-1486, 1993.

[51] K. O. Hill, B. Malo, F. Bilodeau, D. C. Johnson, and J. Albert, "Bragg gratings fabricated in mono-mode photosensitive optical fiber by UV exposure through a phase mask", Appl. Phys. Lett., vol. 62, no. 10, pp. 1035-1037, 1993.

[52] F. Ouellette, "Dispersion cancellation using linearly chirped Bragg grating filters in optical waveguides," Opt. Lett., vol. 12, no. 10, pp. 847-849, 1987.

[53] M. Artiglia, "Upgrading installed systems to multi-gigabit bit-rates by means of dispersion compensation," in ECOC'96, Technical Digest, page 175 , 1996.

[54] R. Kashyap, "On the dispersion of chirped fibre Bragg gratings," in ACOFT'98 Proceedings, page 65,1998.

[55] D. Bayart, B. Clesca, and L. Hamon, "Experimental investigation of the gain flatness characteristics for 1.55 μ m erbium-doped fluoride fiber", IEEE Photon. Technol. Lett., vol. 6, pp. 613-615, 1994.

[56] T. Nakazawa, M. Doi, S. Taniguchi, Ytakasu, and M. Seino, "TiLi:NbO_3 AOTF for 0.8 nm channel-spaced WDM systems", OFC'98, Post-deadline Paper, PD1, 1998.

[57] A. M. Vengsarkar, J. R. Pedrazzani, J. B. Judkins, and P. J. Lemaire, "Long-period fiber-grating-based gain equalizers", Optics Letters, Vol. 21(5), pp. 336-338, Mar. 1996.

[58] P. F. Wysocki et al., "Erbium-doped fiber amplifier flattened beyond 40 nm using long-period grating," OSA Tech. Digest Series, OFC'97, Dallas, TX, paper PD-2.

[59] R. C. Jones, "A new calculus for the treatment of optical systems. VI. Experimental determination of the matrix", J. Optical Society of America, vol. 37, pp. 110-112, 1947.

[60] D. S. Kliger, J. W. Lewis, and C. E. Randall, *Polarized Light in Optics and Spectroscopy*, Academic Press, 1990.

[61] Born, M. and E. Wolf, *Principles of Optics*, 6th ed. Cambridge University Press, 1997.

[62] C. D. Poole, R. E. Eagner, "Phenomenological approach to polarization dispersion in long single-mode fibers", electronic Letters, vol. 22, pp. 1029-1030, 1986.

[63] TIA/EIA Standard, FOTP-175, "Measurement of polarization dependent loss (PDL) of single-mode fiber optic components", May 1995.

[64] IEC International Standard 1300-3-2, Part 3-2: Examination and measurements – polarization dependence of a single-mode fibre-optic device, April 1995.

[65] B.L. Heffner, "Deterministic and analytically complete measurement of polarization dependent transmission through optical devices", IEEE Photonics Technology Letters, 4, pp. 451-453, 1992.

[66] B. Nyman, "Automated system for measuring polarization-dependent loss", Optical Fiber Communication Conference, OFC 1994,Technical Digest, ThK6, page 230, 1994

[67] S. Schmidt, C. Hentschel, "PDL Measurements Using The HP8169A Polarization Controller", Hewlett-Packard publication No. 5964-9937E, 1995.

[68] C. Hentschel, D. Derickson, "Insertion Loss Measurements", Ch. 9 in *Fiber optic test and measurement*, Ed., D. Derickson, Prentice Hall Inc., pp. 354-358, 1998.

[69] P. Lancaster, M. Tismendtshy, "The theory of matrices with applications", 2nd ed.,

Academic Press, 1985, pp. 181-183, 283-286.

[70] B. L. Heffner, "Automated measurement of polarization mode dispersion using Jones matrix eigenanalysis", IEEE Photon. Technol. Letter. Vol. 4, pp.1066, 1992.

[71] Gisin N et al., "Experimental comparison between two different methods for measuring polarization mode dispersion in singlemode fibers", Electron. Lett., vol. 27, 2292, 1991.

[72] Heffner B. L., "Accurate, automated measurement of differential group delay dispersion and principal state variation using Jones matrix eigenanalysis", IEEE Photon. Tech. Lett., vol. 5, page 814, 1993.

[73] F. Curti, B. Daino, G. de Marchis, and F. Matera, "Statistical treatment of the evolution of the principal states of polarization in singlemode fibers", IEEE J. Lightwave Technol. Vol. 8, pp. pp.1162, 1990.

[74] N. Gisin, "Solutions of the Dynamical Equation for Polarization Dispersion", Opt. Commun. 86, page 371, 1991.

[75] N. Gisin, J. P. Von der Weid, J. P. Pellaus, "Polarization mode dispersion of short and long singlemode fibers", IEEE J. Lightwave Technol., vol. 9, pp. 821, 1991.

[76] Y. Namihira, H. Wakabayashi, "Fiber length dependence of polarization mode dispersion measurements in long-length optical fibers and installed optical submarine cables", J. Opt. Commun., 12, pp. 2-9, 1991.

[77] TIA/EIA standard, FOTP-124, "Polarization-Mode Dispersion Measurement for Single-Mode Optical Fibers by Interferometric Method", Aug. 1996.

[78] P. Martin, G. Leboudec, E. Taufflieb, and H. C. Lefevre, "Opitimized polarization mode dispersion measurement with "π-shifted" white light interferometry", Opt. Fiber Technol., 2, pp. 207-212, 1996.

[79] C. D. Poole et al., "Polarization-dependent pulse compression and broadening due to

polarization dispersion in dispersion-shifted fiber", Optics Letters, Vol. 13, pp. 155-157, 1988.

[80] Y. Namihira et al., "Polarization mode dispersion measurements in optical fibers", Symposium on Optical Fiber Measurements, NIST, Boulder, CO., pp. 145-150, Sept. 1992.

[81] C. D. Poole and D. L. Favin, "Polarization-mode dispersion measurements based on transmission spectra through a polarizer", J. Lightwave Technol., LT-12, pp. 917-929, 1994.

[82] TIA/EIA standard, FOTP-113, "Polarization-mode dispersion measurement for single-mode optical fibers by the fixed analyzer method", Washington, DC: TIA, Feb. 1997.

[83] TIA/EIA standard, FOTP-122, "Polarization-mode dispersion measurement for single-mode optical fibers by Jones matrix eigenanalysis", Sept. 1996.

[84] P. Hernday, Product Document, "Polarization-mode dispersion measurement by the Jones matrix eigenanalysis and wavelength-scanning methods", Hewlett-Packard, Lightwave Operation, Santa Rosa, CA, USA, Jan. 1995.

[85] Y. Namihira et al., "Polarization mode dispersion measurements in 1520 km EDFA system", Electron. Lett., vol.28, pp. 881-882, 1992.

[86] D. Andreciani et al., "Measurement of the group-delay difference between the principal states of the polarization on a low-birefringence terrestrial fiber cable", Opt. Lett., vol. 12, page 844, 1987.

[87] T. Ozeke et al, "Birefringence distribution along fiber length", OFC'96, FA4, page 295, USA, 1996.

[88] P. Hernday, "Dispersion Measurements", ch.12, Fiber Optic Test and Measurement, ed., D. Derickson, Prentice Hall PTR, 1998.

[89] S. Bonino, M. Norgia, E. Riccardi, and M. Schiano, "Measurement of polarization properties of chirped fiber gratings", CSELT Technical Reports, vol. XXVI, 1998.

[90] B. Costa, D. Mazzoni, M. Puleo, and E. Vezzoni, "Phase shift technique for the measurement of chromatic dispersion in optical fibers using LED", IEEE J. Quantum Electron., QE-18(10), pp. 1509-1515,1982.

[91] EIA/TIA FOTP-169, "Chromatic dispersion measurement of singlemode optical fibers by the phase shift method", Washington, DC, Telecommunications Industry Association, 1992.